A Tensor Generalized Weighted Linear Predictor for FDA-MIMO Radar Parameter Estimation

Chao Wen, *Member, IEEE*, Yu Xie, *Member, IEEE*, Zhiwei Qiao, Liyun Xu, and Yuhua Qian, *Member, IEEE*

Abstract—Radar parameter estimation in terms of its range, angle and velocity plays a crucial role in many applications. Multiple-input multiple-output (MIMO) radar with frequency diverse array (FDA) is capable of resolving targets in one directional beam with different ranges and velocities (Doppler shifts). Prevalent methods obtain target parameters in a sequential manner to get rid of exhausted multi-dimensional search, but they suffer from accumulated estimation errors. To tackle this issue, a tensor generalized weighted linear predictor (TGWLP) is devised for FDA-MIMO radar parameter estimation, where the parameters are estimated in a parallel manner. Tensor modeling of multidimensional FDA-MIMO radar signal is developed, so that the joint parameter estimation is casted into multiple-pulse-group version of three-dimensional (3D) HR problem associated to the mixed Swerling model. Pulse-group diversity is exploited to obtain precise velocity estimation. In the presence of targets with some identical parameters, the final estimations of unambiguous slant range, conic angle, and radial velocity of a moving target can be easily obtained after the parallel frequency estimations. Besides, all the parameter pairing is automatically achieved, which is free of the extra burden from pairing process. Furthermore, the identifiability of the proposed joint estimator is analyzed. Finally, theoretical analysis and simulations are included to demonstrate that the proposed approach can achieve improved performance compared to the existing methods.

Index Terms—Joint range-angle-velocity estimation, frequency diverse array, subspace based generalized weighted linear predictor, harmonic retrieval.

I. INTRODUCTION

PARAMETER estimation in terms of its range, angle and radial velocity is one of significant radar tasks [1], [2]. The pertinent radar techniques have attracted increasing attention due to its robustness to adverse weather and night operation for autonomous sensing systems [3], [4]. Since conventional phased-array (PA) beampattern is only angle dependent, it is difficult for PA to resolve targets at different

Chao Wen and Liyun Xu are with the Institute of Big Data Science and Industry, Shanxi University, Taiyuan, 030006, China (e-mail: cwen@sxu.edu.cn; xuliyun@sxu.edu.cn).

Yu Xie and Zhiwei Qiao are with School of Computer and Information Technology, Shanxi University, Taiyuan, 030006, China (e-mail: sxlljcxy@gmail.com; zqiao@sxu.edu.cn).

Yuhua Qian is with the Institute of Big Data Science and Industry, also with Key Laboratory of Computational Intelligence and Chinese Information Processing of Ministry of Education, Shanxi University, Taiyuan, 030006, China (e-mail: jinchengqyh@126.com).

distances by employing a single beampattern. By contrast, frequency diverse array (FDA) enjoys its range-angle-time-dependent beampattern, and serves to suppress jamming and boost joint range-angle detection [5]. FDA employs a small frequency increment across array elements and has a range-angle-time-dependent beampattern with coherent waveform [6]. Different from PA and frequency scanning arrays, FDA provides continuous beam scanning without phase shifters or vector modulators [7] and enjoys controllable degree-of-freedom (DOFs) in space, time, frequency and modulation domains. By virtue of its advantages, FDA has wide applications, such as high-resolution imaging [8], multipath mitigation [1], target tracking and localization [9].

Due to the fact that PA is fixed beam steering with a single direction for all ranges, the range estimation from PA beamforming output suffers from the inherent ambiguity problem. The staggered pulse repetition frequency (PRF) is able to mitigate the range ambiguity, but it may bring difficulty to the coherent processing in Doppler domain [10]. The multiple fixed PRF technique favors coherent processing but it is hard to get rid of ghost targets generated in association process [11]. Multiple-input multiple-output (MIMO) radar is a flexible technique, which enjoys higher DOFs in both temporal and spatial domains. Although distributed MIMO radar has been suggested for unambiguous localization, phase synchronization is a real challenge [12]. For colocated MIMO radar, range-angle estimation has been achieved by a transmit subaperture optimization, where the range ambiguity could be overcome [13]. The theoretical performance analysis for FDA-MIMO radar has been made in [14], where MUSIC-based range-angle estimator has been proposed. It has been revealed that a high pulse repetition frequency (PRF) can be used to alleviate the Doppler ambiguity but would incur difficulty in mitigating the range ambiguity especially for the airborne radar systems [15]. A minimum variance distortion-less response (MVDR) based range-angle estimation method has been proposed in [16], which solves the range ambiguity problem caused by the single high PRF. This indicates that the FDA framework is able to simultaneously alleviate the Doppler and range ambiguities with only a single PRF. In addition, the velocity can be determined while the range ambiguous clutter is mitigated, but multi-dimensional search is necessary for the three-dimensional (3D) localization [17]. To reduce the high complexity induced by multi-dimensional search, an unstructured model based method is proposed in [18] where 3D localization is decomposed into three sequential search problems. These estimation methods share the similar way that the estimated value of current parameter will be used for next

parameter estimation. However, the sequential estimation may lead to the estimation errors which may accumulate in the whole process.

This problem can be alleviated by exploring the multi-dimensional structure of the array measurement. Unlike the traditional matrix signal processing approaches, tensor signal processing could enhance array radar performance by exploiting multi-dimensional association information [19], [20], [21]. Parallel factor (PARAFAC) based parameter estimation is prevalent, which benefits from iterative techniques, for example, alternating least squares. According to [19], PARAFAC based methods might not guarantee convergence to the global optimum and require some initialization technique. Tucker3 model based parameter estimation has recently attracted much attention [22], which can improve multi-dimensional subspace-based parameter estimation by using the higher-order singular value decomposition (HOSVD) [20] and low-rank approximations. Pertinent applications of multi-dimensional harmonic retrieval (HR) [23] to MIMO radar has been considered in [24] where two-dimensional angle estimation is achieved via the PARAFAC algorithm. Another potential approach to the multi-dimensional HR problem is subspace based parameter estimation scheme. Tensor ESPRIT (TE) [25], Unitary Tensor ESPRIT (UTE) [19] and Improved multi-dimensional folding (IMDF) [26], [27] can handle multi-dimensional parameter estimation in the presence of identical parameter, but they may not be able to achieve optimal estimation performance. Tensor principal-singular-vector utilization for modal analysis (PUMA) [22] can achieve attractive performance, which benefits from the rank-1 property of the noisy data matrix and linear predictor (LP) with weighted least squares (WLS) techniques. Note that the PUMA based algorithm may not work well when there are identical parameters in one or more dimensions [27]. It is shown that the high resolution of targets with some identical parameters is a challenging problem especially in the presence of deceptive jamming [28], [29], [30].

To alleviate the accumulation error, joint parameter estimation for FDA-MIMO radar is first casted into a multi-dimensional HR problem. The tensor modeling of FDA-MIMO radar signal is featured with a mixed Swerling target model for radar cross section (RCS). In the mixed Swerling case, the RCS of the target should be constant within each pulse group but varying among different pulse groups. Pulse-group diversity is exploited to obtain precise velocity estimation. Unambiguous range estimation can be obtained by range dependence compensation. Furthermore, a tensor generalized weighted linear predictor (TGWLP) is proposed to improve the parameter estimator for targets with some identical parameters. In TGWLP, a complex weighting scheme is devised for the estimation of array steering tensor and a subspace based generalized weighted linear predictor (GWLP) is developed to improve the frequency estimation. The final estimates of unambiguous slant range, conic angle, and radial velocity of a moving target can be easily obtained in a parallel manner. Besides, all the parameter pairings are automatically achieved, which is free of the extra burden from pairing process. The identifiability of the proposed method for joint parameter

estimation is analyzed, which is one significant indicator to determine the maximum number of resolvable target signal components. Our analysis is based on the multiple-pulse-group version of 3D HR problem associated to the mixed Swerling model, rather than typical 3D HR problem associated to the Swerling I model. According to the analysis, the identifiability bound should increase as the number of pulse groups increases until it reaches a threshold.

The main contributions of this paper are listed as follows:

1) We formulate the tensor model of FDA-MIMO radar signal, where a more generalized Swerling target model is established for joint parameter estimation. Thus, we can not only obtain precise velocity estimation by exploiting pulse-group diversity, but also obtain unambiguous range estimation by range dependence compensation.
2) We propose TGWLP to improve the parameter estimates of targets with some identical parameters. In TGWLP, the estimate of array steering tensor is first improved via a complex weighting scheme, and then the parallel frequency estimation is obtained by a subspace based GWLP. Finally, the estimates of range, angle and velocity are efficiently obtained from the estimated frequencies and all the parameters are automatically paired.
3) We make an analysis of the identifiability of the proposed method for joint parameter estimation, which is based on the multiple-pulse-group version of 3D HR problem associated to the mixed Swerling model, rather than typical 3D HR problem associated to the Swerling I model.

The rest of this paper is organized as follows. In Section II, the signal model of forward-looking FDA-MIMO radar is formulated. In Section III, the tensor data model for joint range-angle-velocity estimation is then established after the preprocessing procedures like range compensation. In Section IV, the proposed framework of tensor based multi-dimensional parameter estimation is presented, and the joint range-angle-velocity estimation via TGWLP without parameter pairing is illustrated. Besides, the complexity and identifiability of TGWLP are given and the benchmark to assess unbiased estimators for the FDA-MIMO radar ia derived. Extensive simulation results are presented in Section V. Finally, conclusions are drawn in Section VI.

Notation: Scalars, vectors, matrices and tensors are denoted by italic, bold lower-case, bold upper-case and bold calligraphic symbols, respectively. The angle of a complex number a is written as $\angle(a)$. $|\cdot|$ denotes the complex modulus. $diag(\boldsymbol{y})$ is a diagonal matrix that holds the entries of the vector $\boldsymbol{y}$ on its diagonal. $(\cdot)^T$, $(\cdot)^H$, $(\cdot)^{-1}$, $\otimes$, $\odot$, $\circ$, $.*$ and $./$ denotes the transpose operation, the conjugate transpose operation, inverse operation, the Kronecker product, the Khatri-Rao product, the Hadamard (elementwise) product and the elementwise division, respectively. A tensor of size $N_1 \times N_2 \times \cdots \times N_D$ is denoted by a calligraphic letter $\boldsymbol{\mathcal{Y}}$, and its elements are denoted by $\boldsymbol{\mathcal{Y}}_{n_1,n_2,...,n_D}$. The ηth unfolding of the tensor $\boldsymbol{\mathcal{Y}}$ is written as $[\boldsymbol{\mathcal{Y}}]_{(\eta)} \in \mathbb{C}^{N_\eta \times (N_1 N_2 \cdots N_{\eta-1} N_{\eta+1} \cdots N_D)}$ where the order of the columns is chosen according to [31]. The η-mode product of tensor $\boldsymbol{\mathcal{Y}}$ and matrix $\boldsymbol{U} \in \mathbb{C}^{M_\eta \times N_\eta}$
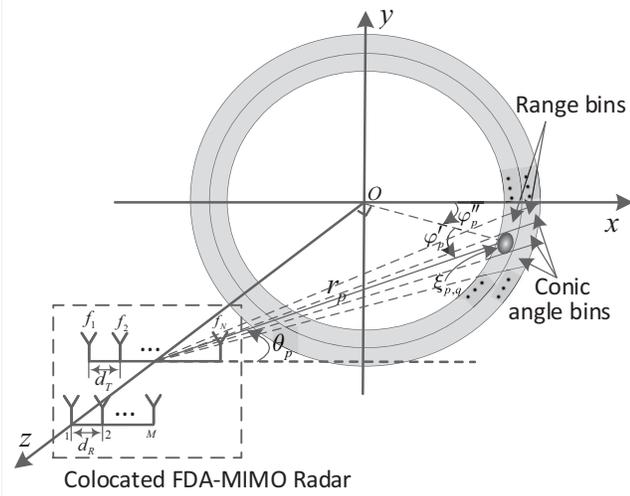
Fig. 1. Forward-looking collocated FDA-MIMO radar geometry.

along the ηth dimension is expressed as $\mathcal{B} = \mathcal{Y} \times_\eta U \in \mathbb{C}^{N_1 \times N_2 \times \cdots \times N_{\eta-1} \times M_\eta \times N_{\eta+1} \times \cdots \times N_D}$. The symbol $\sqcup_\eta$ represents the concatenation operator where $\mathcal{Y} = \mathcal{Y}_1 \sqcup_\eta \mathcal{Y}_2$ is obtained by stacking $\mathcal{Y}_2 \in \mathbb{C}^{N_1 \times N_2 \times \cdots \times N_{\eta-1} \times L_2 \times N_{\eta+1} \times \cdots \times N_D}$ to the end of $\mathcal{Y}_1 \in \mathbb{C}^{N_1 \times N_2 \times \cdots \times N_{\eta-1} \times L_1 \times N_{\eta+1} \times \cdots \times N_D}$ along the ηth dimension. $\lceil \cdot \rceil$ stands for integer ceiling, and $\lfloor \cdot \rfloor$ stands for integer floor.

II. SIGNAL MODEL OF FDA-MIMO RADAR

Consider a narrowband MIMO radar system with N_1 transmit antennas and N_2 receive antennas. The interspacing between transmit antennas is denoted as d_T and similarly that of receive antennas as d_R. The first element is chosen as the reference point. Fig. 1 shows the geometry of the forward-looking collocated FDA-MIMO radar. The target is assumed to be located at xoy plane. The range bins stand for the grids along the slant range. The conic angle θ stands for the angle between the incident ray and the axis of the antenna array. The elevation angle φ'' denotes the angle between zox plane and antenna array. The base angle φ' denotes the angle between xoy plane and incident ray. We have the following assumptions regarding an arbitrary target:

A1 The conic range r_p is much larger than the apertures of the FDA-MIMO radar, so a target is modeled as a point-source in the far-field [6] with the electromagnetic wave independently propagating in the free space.

A2 The relationship among conic angle $\{\theta_p\}_{p=1}^P$, base angle $\{\varphi'_p\}_{p=1}^P$ and elevation angle $\{\varphi''_p\}_{p=1}^P$ can be written as: $\cos(\theta_p) = \cos(\varphi'_p)\cos(\varphi''_p)$.

A3 N_1 transmitted waveforms $\{s_{n_1}(t)\}_{n_1=1}^{N_1}$ are mutually orthogonal and the narrowband transmitted signal of the n_1th element can be expressed as:

$$s_{n_1}(t) = \sqrt{\frac{E}{N_1}}\phi_{n_1}(t)e^{j2\pi f_T(n_1)t}, n_1 = 1, 2, \ldots, N_1,$$

$$(1)$$

where $f_T(n_1)$ denotes the carrier frequency at the n_1th antenna, ϕ_n denotes the unity-energy waveform, i.e.,

$\int_0^{T_P} \phi_{n_i}(t)\,conj\,(\phi_{n_i}(t))dt = 1$, E is the total transmitted energy and the waveforms satisfy the orthogonality condition, that is

$$\int_0^{T_P} \phi_{i_1}(t)conj(\phi_{i_2}(\tau - t))e^{j2\pi\Delta f(i_1-i_2)t}dt = 0,$$
$$i_1, i_2 = 1, 2, \ldots, N_1, i_1 \neq i_2, \qquad (2)$$

where the notation $conj(\cdot)$ stands for the conjugate operator, τ is the time shift within the pulse with $\tau <= T_P/N_1$, T_P denotes the pulse repetition interval (PRI).

A4 The carrier frequency at the n_1th antenna satisfies $f_T(n_1) = f_C + (n_1 - 1)\Delta f$, $n_1 = 1, 2, \ldots, N_1$, where the frequency increment Δf is negligible compared with the carrier frequency f_C, i.e., $f_C \gg \Delta f$.

A5 A total of Q probing pulses are regarded as Q_g pulse groups. The RCS is constant within each group, but it varies from pulse group to pulse group. In this scenario, the mixture of Swerling I and II target models with nondispersive propagation medium [24] is considered.

According to [32], the range bin interval (receive array sampling interval) can be shorter than the range resolution unit determined by the signal bandwidth B, the conic angle bin interval (antenna scanning step) can be smaller than the beamwidth. The total number of range bins is determined by the product of sampling rate f_s and PRI T_P.

The range resolution, the Doppler resolution, the maximum unambiguous Doppler frequency and the maximum unambiguous range can be determined. According to [33], the traditional range resolution and Doppler resolution are determined by $c/2B$ and $f_{PRF}Q_g/Q$, respectively, with f_{PRF} being PRF and $f_C \gg B \gg f_{PRF}$. The maximum unambiguous Doppler frequency is f_{PRF}. The maximum unambiguous range $r_{p_{max}}$ equals $c/2f_{PRF}$. In the following, we consider colocated FDA-MIMO radar transmitting only one PRF to solve the multi-dimensional parameter estimation problem in the presence of multiple moving targets with range ambiguity.

A. Received Signal Model

Without loss of generality, multi-target case of joint range-angle-velocity estimation for FDA radar is considered, which can be regarded as a more generalized version of the array signal model in [16] and [18]. For an arbitrary target, the signal received by the n_2th element can be written as:

$$\begin{aligned}
x_{n_2} &= \sum_{p=1}^P \sum_{n_1=1}^{N_1} \sqrt{\frac{E}{N_1}}\xi_p\phi_{n_1}(t - \tau_{n_1,n_2,p}) \\
&\quad \times e^{j2\pi(f_T(n_1)+f_D(p,n_1))(t-\tau_{n_1,n_2,p})} \\
&= \sum_{p=1}^P \sum_{n_1=1}^{N_1} \sqrt{\frac{E}{N_1}}\xi_p\phi_{n_1}(t - \tau_{n_1,n_2,p}) \\
&\quad \times e^{j2\pi f_D(p)(t-\tau_{n_1,n_2,p})}e^{j2\pi f_T(n_1)(t-\tau_{n_1,n_2,p})}
\end{aligned}$$

$$(3)$$

where ξ_p denotes RCS of the pth target, $\tau_{n_1,n_2,p} = [2r_p - d_T(n_1-1)\cos(\theta_p) - d_R(n_2-1)\cos(\theta_p)]/c$ denotes the transmit plus receive time delays, $f_D(p, n_1)$ denotes the Doppler frequency, i.e., $f_D(p, n_1) = 2v_p/\lambda_{n_1}$, v_p is the radial velocity of the pth target, $\lambda_{n_1} = c/f_T(n_1)$ is the wavelength

corresponding to the n_1th transmit antenna and $\lambda_0 = c/f_C$ is the reference wavelength. Actually, the Doppler frequency corresponding to the pth target can be approximately expressed as $f_D(p) = 2v_p/\lambda_0$ since the frequency increment is negligible compared with the carrier frequency.

The measurement data are down converted, matched filtered and stored in the receive array. The matched filters yield outputs correspond to isolated propagation paths from transmitters to receivers. After matched filtering by $\phi_{n_1}(t)e^{j2\pi\Delta ft}$ [16], the n_1th output of the n_2th received antenna can be expressed as:

$$
\begin{aligned}
x_{n_2,n_1} &\approx \sum_{p=1}^{P} \sqrt{\frac{E}{N_1}}\xi_p e^{j2\pi f_D(p)(t-2r_p/c)}e^{-j4\pi\frac{f_T(n_1)}{c}r_p} \\
&\quad \times e^{j2\pi\frac{f_T(n_1)}{c}[d_T(n_1-1)\cos(\theta_p)+(n_2-1)2\pi d_R\cos(\theta_p)]} \\
&\approx \sum_{p=1}^{P} \sqrt{\frac{E}{N_1}}\xi_p e^{j2\pi f_D(p)(t-2r_p/c)}e^{-j4\pi f_C r_p/c} \\
&\quad \times e^{j(n_1-1)2\pi[f_C d_T\cos(\theta_p)-2\Delta f r_p]/c}e^{j(n_2-1)2\pi d_R\cos(\theta_p)/\lambda_0}
\end{aligned}
\tag{4}
$$

The approximation in (4) is obtained since the frequency increment is relatively negligible [34].

It is well known that the RCS is constant during the CPI in Swerling I target model, while it varies from pulse to pulse in Swerling II target model. The common idea is shared that the Swerling models are employed to approximate and simplify the RCS variation during a processing time. In order to unify the two Swerling cases, the RCS is assumed to be constant during each small part of the whole processing time but it varies from part to part. In this sense, the whole processing time is equivalent to the combination of many short CPIs in practice. Therefore, our assumption is based on the coexisting of Swerling I and II cases which can be easily proved. In the mixed Swerling case, the RCS is constant within each pulse group, but it varies among different pulse groups. Let $q = 1, 2, \ldots, Q_g$ and $n_3 = 1, 2, \ldots, N_3$ ($N_3 = Q/Q_g$) denote the indices of the pulse groups and the pulses within each group, respectively. We define $t = (q-1)N_3 T_P + (n_3-1)T_P$ and (4) can be further expressed as:

$$
\begin{aligned}
x_{n_2,n_1,n_3,q} &= \sum_{p=1}^{P}\sqrt{\frac{E}{N_1}}\xi_p(q)e^{j(n_3-1)2\pi f_D(p)T_P} \\
&\quad \times e^{j(n_1-1)2\pi[f_C d_T\cos(\theta_p)-2\Delta f r_p]/c}e^{j(n_2-1)2\pi d_R\cos(\theta_p)/\lambda_0}
\end{aligned}
\tag{5}
$$

The term $e^{j2\pi f_D(p)[(q-1)N_3 T_P - 2r_p/c]}e^{-j4\pi f_C r_p/c}$ in (5) is absorbed into $\xi_p(q)$ which varies among different pulse groups and herein we do not include the term for the sake of simplicity.

B. Received Data in Vector Form

According to (5), the virtual data snapshot can be expressed in vector form:

$$
\tilde{\boldsymbol{x}}(n_3,q) = \sum_{p=1}^{P}\sqrt{\frac{E}{N_1}}\xi_p(q)c_p(n_3)(\boldsymbol{a}(r_p,\theta_p)\otimes\boldsymbol{b}(\theta_p)) \\
+ \boldsymbol{z}(n_3,q)
\tag{6}
$$

where $\xi_p(q)$ accounts for the RCS in mixed Swerling case, $c_p(n_3) = e^{j(n_3-1)2\pi f_D(p)T_P}$ accounts for the Doppler effect within the each pulse group, $\boldsymbol{z}(n_3,q)$ denotes the noise term, $\boldsymbol{A}(r,\theta) = [\boldsymbol{a}(r_1,\theta_1),\boldsymbol{a}(r_2,\theta_2),\ldots,\boldsymbol{a}(r_P,\theta_P)] \in \mathbb{C}^{N_1\times P}$ is transmit steering matrix, $\boldsymbol{B}(\theta) = [\boldsymbol{b}(\theta_1),\boldsymbol{b}(\theta_2),\ldots,\boldsymbol{b}(\theta_P)] \in \mathbb{C}^{N_2\times P}$ is receive steering matrix, $\boldsymbol{b}(\theta)$ and $\boldsymbol{a}(r,\theta)$ are the receive and transmit steering vectors, respectively, defined as:

$$
\boldsymbol{b}(\theta_p) = \left[1, e^{j2\pi\frac{d_R}{\lambda_0}\cos(\theta_p)}, \ldots, e^{j2\pi\frac{d_R}{\lambda_0}(N_2-1)\cos(\theta_p)}\right]^T
\tag{7}
$$

$$
\boldsymbol{a}(r_p,\theta_p) = \boldsymbol{r}(r_p) .* \boldsymbol{d}(\theta_p)
\tag{8}
$$

where $\boldsymbol{r}(r_p) = [1, e^{-j4\pi\Delta f r_p/c}, \ldots, e^{-j4\pi\Delta f(N_1-1)r_p/c}]^T$ is the transmit range steering vector and $\boldsymbol{d}(\theta_p) = [1, e^{j2\pi d_T\cos(\theta_p)/\lambda_0}, \ldots, e^{j2\pi d_T(N_1-1)\cos(\theta_p)/\lambda_0}]^T$ is the transmit angular steering vector. For the frequency increment is zero, the array model in (6) can be simplified to the conventional MIMO radar with fixed carrier frequency [24]. Since the transmit steering vector in (8) is not only angle-dependent but also range-dependent, the FDA-MIMO radar could utilize the joint transmit and receive degrees of freedom to determine the range and angle parameters.

III. DATA MODEL FOR JOINT RANGE-ANGLE-VELOCITY ESTIMATION

A. Range Dependence Compensation

FDA-MIMO radar benefits from transmit steering vector and provides resolvability in range. For the high PRF radar, the true range of the pth target in presence of range ambiguity is written as:

$$
r_p = r_{p_0} + (k_p-1)r_{p_{\max}}, k_p = 1, 2, \ldots, K
\tag{9}
$$

where r_{p_0} is the principal range of the target which is also the ambiguous range according to [16], k_p is the index of range ambiguity of the target, K denotes the number of ambiguous ranges, $r_{p_{\max}} = c/(2f_{PRF})$ denotes the maximum unambiguous range.

Traditionally, the range estimate falls within some adjacent range resolution cell and the range estimation accuracy is limited by the signal bandwidth. However, range estimation accuracy can be further improved by range dependence compensation on the received data. The compensation is implemented range by range, followed by the principal range difference estimation. Note that the priori range estimate $\breve{r}$ approximately equals the principal range. The principal range difference is defined as:

$$
\Delta r_p = r_{p_0} - \breve{r}_p
\tag{10}
$$

where $\breve{r}_p$ is the priori range estimate, which is also the priori ambiguous range estimate and can be calculated with the range bin number and bin size, the principal range difference Δr_p is relatively small and falls within a single range resolution cell, which can be regarded as a random variable uniformly distributed between $[-c/4B, c/4B]$. Thus, the range compensating vector can be expressed as:

$$
\boldsymbol{h}_{\boldsymbol{1}_{N_2}} = \boldsymbol{h}(\breve{r}_p) \otimes \boldsymbol{1}_{N_2}
\tag{11}
$$

where $\boldsymbol{h}\left(\breve{r}_p\right) = \left[1, e^{j2\pi\frac{2\Delta f}{c}\breve{r}_p}, \ldots, e^{j2\pi\frac{2\Delta f}{c}(N_1-1)\breve{r}_p}\right]^T$, $\boldsymbol{1}_{N_2}$ denotes the vector with all elements being equal to one. After compensation, the received data in (6) can be expressed as (12) where $\tilde{r}_p = \Delta r_p + (k_p - 1)r_{p_{\max}}$. It can be concluded that range estimation is equivalent to estimating k_p and Δr_p. Since the principal range difference Δr_p is relatively small and falls within a single range resolution cell, the compensated range frequency of the target in FDA-MIMO radar can be viewed as a shift of the range frequency of traditional MIMO by a factor corresponding to the index of range ambiguity. The index of range ambiguity can be estimated accurately by MVDR based approach when the frequency increment is carefully selected [16]. With the index determined, estimation accuracy of the range and the other parameters can be further improved via tensor modeling.

B. Data Tensor Model for Joint Range-Angle-Velocity Estimation

In [16] and [18], data matrices are single-target oriented and multiple dimensional parameters are sequentially estimated. By contrast, parallel parameter estimation based on multiple-target oriented data tensor model in mixed Swerling case is studied in this paper. Before that, we build a compact multi-target oriented data model. According to (12), the total received data after the compensation can be written in the following four-order tensor form:

$$\boldsymbol{\mathcal{Y}} = \tilde{\boldsymbol{\mathcal{X}}} + \tilde{\boldsymbol{\mathcal{Z}}} \tag{13}$$

where the noise free tensor $\tilde{\boldsymbol{\mathcal{X}}} \in \mathbb{C}^{N_1 \times N_2 \times N_3 \times Q_g}$ has entries of the form:

$$\tilde{\mathcal{X}}_{n,m,l,q} = \sum_{p=1}^{P} \xi_p\left(q\right) e^{j(n_1-1)\omega_{1,p}} e^{j(n_2-1)\omega_{2,p}} e^{j(n_3-1)\omega_{3,p}} \tag{14}$$

where $\omega_{1,p} = 2\pi\left[d_T f_C \cos\left(\theta_p\right) - 2\tilde{r}_p\Delta f\right]/c$ relies on both range and angle, $\omega_{2,p} = 2\pi d_R f_C \cos\left(\theta_p\right)/c$ and $\omega_{3,p} = 4\pi v_p T_P/\lambda_0$ are dependent on angle and velocity, respectively, the observed tensor $\boldsymbol{\mathcal{Y}}$ and the noise tensor $\tilde{\boldsymbol{\mathcal{Z}}}$ are of size $N_1 \times N_2 \times N_3 \times Q_g$. $\tilde{\boldsymbol{\mathcal{Z}}}$ represents the additive noise component inherent in the measurement process, which can be modeled as a zero-mean random process that is uncorrelated in all dimensions.

The decomposition in (14) is also known as a multi-dimensional HR problem, where the data representation for unambiguous estimation allows more efficiency in the extraction of joint range-angle-velocity information. The measurement data is modeled as a superposition of undamped exponentials sampled on a 3D grid at Q_g pulse-groups of intervals. The data is sampled on a four-dimensional lattice, so the 3D parameter estimation is casted into a multiple-pulse-group version of the 3D HR problem [24]. Note that conventional methods suffer from the accumulated estimation errors due to the sequential frequency estimation from the matrix or vector. To overcome this problem, our method focus on the parallel frequency estimation from the data tensor in (13). With the estimated frequencies $\{\hat{\omega}_{\eta,p}\}$ in IV-B, the angle and velocity are computed according to (14) as:

$$\hat{\theta}_p = \text{acos}(\frac{\hat{\omega}_{2,p}c}{2\pi d_R f_C}) \tag{15}$$

$$\hat{v}_p = \frac{\hat{\omega}_{3,p}\lambda_0}{4\pi T_P} \tag{16}$$

With $\hat{k}_p$ obtained in the similar way to [16], the principal range difference is then estimated as follows:

$$\Delta\hat{r}_p = \frac{d_T f_C \cos(\hat{\theta}_p)}{2\Delta f} - \frac{\omega_{1,p}c}{4\pi\Delta f} - (\hat{k}_p - 1)r_{\max} \tag{17}$$

The whole algorithm of the multi-dimensional parameter estimation is summarized at the end of IV-B.

IV. TENSOR GENERALIZED WEIGHTED LINEAR PREDICTOR BASED ESTIMATOR

In this section, a tensor generalized weighted linear predictor (TGWLP) based estimator is proposed. The main procedure and derivation of TGWLP based estimator are given in section IV-A, where the complexity is also anylized. The performance degradation problem in the presence of identical or close frequencies are alleviated by the complex weighting optimization, which is illustrated in section IV-B. Then, the indicator to determine the maximum number of resolvable components for the proposed method is given in IV-C. Finally, the benchmark to assess the unbiased parameter estimators for FDA-MIMO radar is studied in IV-D.

A. Tensor based Multi-dimensional Parameter Estimation

According to the structure of the data (14), a generalized noise-free data tensor $\boldsymbol{\mathcal{X}} \in \mathbb{C}^{N_1 \times N_2 \times \cdots \times N_D \times Q_g}$ with Q_g pulse groups can be expressed as:

$$\boldsymbol{\mathcal{X}} = \boldsymbol{\mathcal{I}}_P^{D+1} \times_1 \boldsymbol{G}^{(1)} \times_2 \boldsymbol{G}^{(2)} \cdots \times_D \boldsymbol{G}^{(D)} \times_{D+1} \boldsymbol{G}^{(D+1)} \tag{18}$$

$$
\begin{aligned}
\boldsymbol{y}\left(n_3, q\right) &= \tilde{\boldsymbol{x}}\left(n_3, q\right) .* \boldsymbol{h_1}_{N_2} \\
&= \left[\sum_{p=1}^{P}\sqrt{\frac{E}{N_1}}\xi_p(q)c_p(n_3)(\boldsymbol{a}(r_p,\theta_p)\otimes\boldsymbol{b}(\theta_p)) + \boldsymbol{z}(n_3,q)\right] .* \boldsymbol{h_1}_{N_2} \\
&= \sum_{p=1}^{P}\sqrt{\frac{E}{N_1}}\xi_p\left(q\right)c_p\left(n_3\right)\left(\boldsymbol{r}\left(r_p\right).*\boldsymbol{d}\left(\theta_p\right).*\boldsymbol{h}\left(\breve{r}_p\right)\right)\otimes\boldsymbol{b}\left(\theta_p\right) + \boldsymbol{z}\left(n_3,q\right).*\boldsymbol{h_1}_{N_2} \\
&= \sum_{p=1}^{P}\sqrt{\frac{E}{N_1}}\xi_p\left(q\right)c_p\left(n_3\right)\left(\boldsymbol{r}\left(\tilde{r}_p\right).*\boldsymbol{d}\left(\theta_p\right)\right)\otimes\boldsymbol{b}\left(\theta_p\right) + \boldsymbol{z}\left(n_3,q\right).*\boldsymbol{h_1}_{N_2}
\end{aligned}
\tag{12}
$$

where $\mathcal{I}_P^{D+1} \in \mathbb{C}^{P \times P \times \cdots \times P}$ denotes a $(D+1)$-dimensional tensor whose $(p, p, \cdots, p)$ entry equals 1 and zero otherwise.

$$\boldsymbol{G}^{(\eta)} = \begin{bmatrix} \boldsymbol{g}_1^{(\eta)} & \boldsymbol{g}_2^{(\eta)} & \cdots & \boldsymbol{g}_P^{(\eta)} \end{bmatrix}, \qquad (19)$$

$$\boldsymbol{g}_p^{(\eta)} = \begin{bmatrix} 1 & e^{j\omega_{\eta,p}} & \cdots & e^{j(N_\eta-1)\omega_{\eta,p}} \end{bmatrix}^T, \\ \eta = 1, 2, \ldots, D, \qquad (20)$$

$$\boldsymbol{g}_p^{(D+1)} = \begin{bmatrix} \xi_p(1) & \xi_p(2) & \cdots & \xi_p(Q_g) \end{bmatrix}. \qquad (21)$$

On the other hand, the HOSVD of the noise-corrupted $\mathcal{X}$ can be written as the following product:

$$\mathcal{Y} = \mathcal{S} \times_1 \boldsymbol{U}^{(1)} \times_2 \boldsymbol{U}^{(2)} \cdots \times_D \boldsymbol{U}^{(D)} \times_{D+1} \boldsymbol{U}^{(D)} \qquad (22)$$

where $\mathcal{S} \in \mathbb{C}^{N_1 \times N_2 \times \cdots \times N_D \times Q_g}$ is the core ordered tensor satisfying the property of all-orthogonality, $\boldsymbol{U}^{(\eta)}$ is the unitary matrix containing the ηth mode singular vectors [31].

Since $\mathcal{Y}$ is of rank P, it can be estimated by using the truncated HOSVD [31]:

$$\mathcal{Y} = \mathcal{S}_s \times_1 \boldsymbol{U}_s^{(1)} \times_2 \boldsymbol{U}_s^{(2)} \times \cdots \times_D \boldsymbol{U}_s^{(D)} \times_{D+1} \boldsymbol{U}_s^{(D+1)} \qquad (23)$$

where $\mathcal{S}_s$ has only the first M_η elements of $\mathcal{S}_s$ in the ηth dimension and $\boldsymbol{U}_s^{(\eta)}$ contains the first M_η dominant singular vectors of $\boldsymbol{U}_s^{(\eta)}$ with $M_\eta = \min\{P, N_\eta, \bar{N}Q_g/N_\eta\}$, $M_{D+1} = \min\{P, \bar{N}\}$ and $\bar{N} = \prod_{\eta=1}^D N_\eta$. The tensor-based signal subspace of $\mathcal{Y}$ can be expressed as [19]:

$$\mathcal{U}_s = \mathcal{S}_s \times_1 \boldsymbol{U}_s^{(1)} \times_2 \boldsymbol{U}_s^{(2)} \times \cdots \times_D \boldsymbol{U}_s^{(D)} \in \mathbb{C}^{N_1 \times N_2 \times \cdots \times N_D \times P} \qquad (24)$$

According to [26], when $P \leq \min\{Q_g, \bar{N}\}$, $[\mathcal{U}_s]_{(D+1)}^T$ has P columns that together span the same column space of $[\mathcal{Y}]_{(D+1)}^T$. The column space is also spanned by $[\mathcal{G}_s]_{(D+1)}^T$ where the array steering tensor $\mathcal{G}_s \in \mathbb{C}^{N_1 \times N_2 \times \cdots \times N_D \times P}$ is expressed as:

$$\mathcal{G}_s = \mathcal{I}_P^{D+1} \times_1 \boldsymbol{G}^{(1)} \times_2 \boldsymbol{G}^{(2)} \cdots \times_D \boldsymbol{G}^{(D)} \\ = \mathcal{G}_{s1} \sqcup_{D+1} \mathcal{G}_{s2} \sqcup_{D+1} \cdots \sqcup_{D+1} \mathcal{G}_{sP} \qquad (25)$$

where the tensor $\mathcal{G}_s$ in (25) has been expressed as concatenated subtensors $\{\mathcal{G}_{sp}\}_{p=1}^P$ and each of the concatenated subtensors is featured with only single tone. The subtensor $\mathcal{G}_{sp}$ in (25) is further expressed as:

$$\mathcal{G}_{sp} \approx \varepsilon_p \boldsymbol{g}_p^{(1)} \circ \boldsymbol{g}_p^{(2)} \circ \cdots \circ \boldsymbol{g}_p^{(D)}, p = 1, 2, ..., P \qquad (26)$$

with $\{\varepsilon_p\}$ being unknown complex scalars. The model in (26) aims to express how the concatenated subtensor is decomposed into D-dimensional component of the single tone. Thus, the linear prediction property of each dimensional component can be exploited afterwards. Note that it is different from the parameter estimation based on the typical PARAFAC model where the iterative techniques require many iterations and tolerable initialization [19]. The proposed estimator based on HOSVD can alleviate the problem. There exists the linear prediction property of $\boldsymbol{g}_p^{(\eta)}$, so a system of linear equations of $\{\rho_{\eta,p}\}$ can be obtained as:

$$g_{n_\eta}^{(\eta)} \approx \rho_{\eta,p} g_{n_\eta-1}^{(\eta)}, \rho_{\eta,p} = e^{j\omega_{\eta,p}} \qquad (27)$$

where $g_{n_\eta}^{(\eta)}$ denotes the n_ηth element of $\boldsymbol{g}_p^{(\eta)}$, $n_\eta = 2, 3, \ldots, N_\eta$. Under sufficiently small noise conditions, there exists a $P \times P$ nonsingular matrix $\boldsymbol{T}$ such that

$$[\mathcal{U}_s]_{(D+1)} \approx \boldsymbol{T}[\mathcal{G}_s]_{(D+1)} \qquad (28)$$

According to [35], the HOSVD-based methods can obtain the improved estimation of true signal subspace via the high dimensional space projection. It is very possible to lead to smaller effective noise conditions, which makes (28) hold. With the estimated $\boldsymbol{T}$ in subsection IV-B, the estimation of $\mathcal{G}_s$ can be obtained as:

$$\hat{\mathcal{G}}_s \approx \mathcal{U}_s \times_{D+1} \boldsymbol{T}^T \qquad (29)$$

Applying another truncated HOSVD to the subtensor $\mathcal{G}_{sp}$ and yields

$$\mathcal{G}_{sp} \approx \gamma_p \times_1 \boldsymbol{\alpha}_p^{(1)} \times_2 \boldsymbol{\alpha}_p^{(2)} \times \cdots \times_D \boldsymbol{\alpha}_p^{(D)} \qquad (30)$$

where

$$[\mathcal{G}_{sp}]_{(\eta)} \approx \boldsymbol{\alpha}_p^{(\eta)} \gamma_{\eta,p} \boldsymbol{\beta}_p^{(\eta)} \qquad (31)$$

is the rank-1 SVD truncation with $|\gamma_p|^2 = \gamma_{\eta,p}^2$ for any η [23]. Comparing (26) and (30), it is seen that the noise-free $\boldsymbol{\alpha}_p^{(\eta)}$ spans the same subspace as $\boldsymbol{g}_p^{(\eta)}$, meaning that $\boldsymbol{\alpha}_p^{(\eta)} \approx \varepsilon_{\eta,p} \boldsymbol{g}_p^{(\eta)}$ where $\varepsilon_{\eta,p}$ is a complex scalar. There exists the linear prediction property of $\boldsymbol{\alpha}_p^{(\eta)}$ which is similar to that of $\boldsymbol{g}_p^{(\eta)}$ in (26), so a system of subspace based linear equations of $\{\rho_{\eta,p}\}$ can be obtained as:

$$\alpha_{n_\eta}^{(\eta)} \approx \rho_{\eta,p} \alpha_{n_\eta-1}^{(\eta)}, \rho_{\eta,p} = e^{j\omega_{\eta,p}} \qquad (32)$$

where $\alpha_{n_\eta}^{(\eta)}$ denotes the n_ηth element of $\boldsymbol{\alpha}_p^{(\eta)}$, with the linear prediction error being

$$\delta_{\tilde{n}_\eta}^{(\eta)} = \alpha_{p,n_\eta}^{(\eta)} - \tilde{\rho}_{\eta,p} \alpha_{n_\eta-1}^{(\eta)}, \; \tilde{n}_\eta = 1, 2, \ldots, N_\eta - 1 \qquad (33)$$

where $\delta_{\tilde{n}_\eta}^{(\eta)}$ denotes the $\tilde{n}_\eta$th element of complex Gaussian noise vector $\boldsymbol{\delta}^{(\eta)}$ with zero mean and variance σ_η^2, and $\tilde{\rho}_{\eta,p}$ is a variable corresponds to $\rho_{\eta,p}$ which is to be determined.

A GWLP frequency estimator based on the principal left singular vector is further developed to solve the linear prediction problem in (32). The multi-dimensional HR problem is decomposed into the multiple separate solutions of one-dimensional subspace based linear predictions, where the frequencies in all dimensions can be obtained by utilizing the linear prediction property and the weighted least squares. The corresponding estimated frequency, denoted by $\{\hat{\omega}_{\eta,p}\}$, can be obtained as [36]:

$$\hat{\omega}_{\eta,p} = \angle \left((\boldsymbol{J}_{1,\eta} \boldsymbol{\alpha}_p^{(\eta)})^H \boldsymbol{W}^{(\eta)}(\omega_{\eta,p}) \boldsymbol{J}_{2,\eta} \boldsymbol{\alpha}_p^{(\eta)} \right) \qquad (34)$$

where $\boldsymbol{J}_{1,\eta} \boldsymbol{\alpha}_p^{(\eta)}$ and $\boldsymbol{J}_{2,\eta} \boldsymbol{\alpha}_p^{(\eta)}$ are equal-sized selected sub-vectors corresponding to the signal subspace, $\angle$ represents the phase angle operator and the optimum weighting matrix $\boldsymbol{W}^{(\eta)}(\omega_{\eta,p})$ is characterized by the unknown frequency, which has a closed form with the (k_m, k_n)th entries being

$$\left[\boldsymbol{W}^{(\eta)}(\omega_{\eta,p}) \right]_{k_m, k_n} = \frac{N_\eta \min(k_m, k_n) - k_m k_n}{N_\eta} e^{j(k_m - k_n)\omega_{\eta,p}} \qquad (35)$$

where $k_m = 1, 2, \ldots, N_\eta - 1$, $k_n = 1, 2, \ldots, N_\eta - 1$. As the frequency is unknown, an initial frequency estimation of $\{\hat{\omega}_{\eta,p}\}$ is obtained by using weighted linear predictor (WLP) [37], that is,

$$\hat{\omega}_{\eta,p} = \angle \left(\sum_{k_m=1}^{N_\eta - 1} \frac{6}{N_\eta^2 - 1} \alpha_{k_m}^{(\eta)} \left[\boldsymbol{W}^{(\eta)}(\omega_{\eta,p}) \right]_{k_m, k_m} \alpha_{k_m+1}^{(\eta)} \right) \tag{36}$$

Thus, the iterative relaxation procedure of frequency estimation is summarized in Table I. Note that the iterations are set as no more than 2, according to [36], because of no significant improvement for more iterations.

TABLE I
SUBSPACE BASED GENERALIZED WEIGHTED LINEAR PREDICTOR

1)Obtain initial frequency estimation of $\hat{\omega}_{\eta,p}$ from each $\boldsymbol{\alpha}_p^{(\eta)}$ according to (36).
2)Use $\hat{\omega}_{\eta,p}$ to construct optimum weighting matrix $\boldsymbol{W}^{(\eta)}(\omega_{\eta,p})$ from (35).
3)Update the estimation of $\hat{\omega}_{\eta,p}$ using $\boldsymbol{W}^{(\eta)}(\omega_{\eta,p})$ in 2) according to (34).
4)Repeat Steps 2) and 3) until parameter convergence.

In order to achieve a higher estimation accuracy, $\boldsymbol{\mathcal{Y}}$ in Table II can be replaced by the forward-backward (FB) averaging version $\boldsymbol{\mathcal{Y}}^{(FB)}$, which is obtained as:

$$\boldsymbol{\mathcal{Y}}^{(FB)} = \boldsymbol{\mathcal{Y}} \sqcup_{D+1} \boldsymbol{\mathcal{Y}}^* \times \boldsymbol{\Pi}_{N_1} \times \boldsymbol{\Pi}_{N_2} \times \cdots \times \boldsymbol{\Pi}_{Q_g} \tag{37}$$

where $\boldsymbol{\Pi}_{N_\eta}$ symbolizes the $N_\eta \times N_\eta$ matrix with ones in its anti-diagonal and zeros elsewhere. Correspondingly, the algorithm is named as TGWLP-FB.

The major computational complexity of the TGWLP algorithm is studied as follows. Firstly, the HOSVD of $\boldsymbol{\mathcal{Y}}$ involves $(D+1)$ SVDs, which is of $O(\kappa P(D+1)Q_g \prod_{\eta=1}^{D} N_\eta)$, where κ is a constant depending on the design of the algorithm [38]. This step is most computationally demanding but only needs to compute once. Then, the complexity for the truncated HOSVD of P subtensors $\boldsymbol{\mathcal{G}}_{sp} \in \mathbb{C}^{N_1 \times N_2 \times \cdots \times N_D}$, $p = 1, 2, \cdots, P$, is $O(\kappa P \prod_{\eta=1}^{D} N_\eta)$ because contains only one frequency. Finally, the GWLP iterations require only multiplication and addition and their computational complexities are not included. Combining the results, the overall computational requirement is $O(\kappa P(D+1)Q_g \prod_{\eta=1}^{D} N_\eta) + O(\kappa P \prod_{\eta=1}^{D} N_\eta)$. The main complexity of TGWLP-FB remains unchanged while Q_g will be replaced by $2Q_g$, though the tensor size is larger.

B. Complex Weighting based Nonsingular Matrix Estimation

False targets generated by deceptive jammers have similar characteristics with the true target in multiple aspects, including space, time, frequency and Doppler [30], which makes parameter estimation of jammer a significant task in the radar. This calls for the approach to handle identical frequency scenarios. However, the estimation performance degrades in the presence of identical or close frequencies, since the eigenvectors are not linearly independent any more. To address this issue, an optimized complex weighting scheme is proposed, which is similar to [27].

Firstly, subtensors $\boldsymbol{\mathcal{U}}_{s1}$ and $\tilde{\boldsymbol{\mathcal{U}}}_{s2}(\eta)$, $\eta = 1, 2, \ldots, D$, are constructed as:

$$\boldsymbol{\mathcal{U}}_{s1} = \boldsymbol{\mathcal{U}}_s \times_1 \boldsymbol{J}_{1,1} \times_2 \boldsymbol{J}_{1,2} \times \cdots \times_D \boldsymbol{J}_{1,D}$$
$$= \boldsymbol{\mathcal{S}}_s \times_1 \boldsymbol{J}_{1,1} \boldsymbol{U}_s^{(1)} \times_2 \boldsymbol{J}_{1,2} \boldsymbol{U}_s^{(2)} \times \cdots \times_D \boldsymbol{J}_{1,D} \boldsymbol{U}_s^{(D)} \tag{38}$$

$$\tilde{\boldsymbol{\mathcal{U}}}_{s2}(\eta) = \boldsymbol{\mathcal{S}}_s \times_1 \boldsymbol{J}_{1,1} \boldsymbol{U}_s^{(1)} \cdots \times_{\eta-1} \boldsymbol{J}_{1,\eta-1} \boldsymbol{U}_s^{(\eta-1)}$$
$$\times_\eta \boldsymbol{J}_{2,\eta} \boldsymbol{U}_s^{(\eta)} \times_{\eta+1} \boldsymbol{J}_{1,\eta+1} \boldsymbol{U}_s^{(\eta+1)} \cdots \times_D \boldsymbol{J}_{1,D} \boldsymbol{U}_s^{(D)} \tag{39}$$

where

$$\boldsymbol{J}_{1,\eta} = \begin{bmatrix} \boldsymbol{I}_{N_\eta-1} & \boldsymbol{0}_{(N_\eta-1)\times 1} \end{bmatrix} \tag{40}$$

and

$$\boldsymbol{J}_{2,\eta} = \begin{bmatrix} \boldsymbol{0}_{(N_\eta-1)\times 1} & \boldsymbol{I}_{N_\eta-1} \end{bmatrix} \tag{41}$$

are selection matrices. In the absence of noise, we have:

$$\boldsymbol{\mathcal{U}}_{s1} \times_{D+1} \left(\boldsymbol{\Psi}^{(\eta)} \right)^T = \tilde{\boldsymbol{\mathcal{U}}}_{s2}(\eta) \tag{42}$$

where $\boldsymbol{\Psi}^{(\eta)} = \boldsymbol{T}^{(\eta)} \boldsymbol{\Phi}^{(\eta)} \left(\boldsymbol{T}^{(\eta)} \right)^{-1}$ with $\boldsymbol{T}^{(\eta)}$ being a nonsingular matrix and $\boldsymbol{\Phi}^{(\eta)}$ is a diagonal matrix which contains the frequency information:

$$\boldsymbol{\Phi}^{(\eta)} = diag \left(\begin{bmatrix} e^{j\omega_{\eta,1}} & e^{j\omega_{\eta,2}} & \cdots & e^{j\omega_{\eta,P}} \end{bmatrix} \right) \tag{43}$$

In fact, when there exist identical frequencies in one or more dimension, the eigenvectors of $\boldsymbol{\Phi}^{(\eta)}$ are not linearly independent anymore [34], which leads to the unreliable estimation of $\boldsymbol{\mathcal{G}}_s$ and the degraded performance of frequency estimation. To solve this problem, a complex weighting based nonsingular matrix estimation method is utilized. Equal-sized subtensors $\tilde{\boldsymbol{\mathcal{U}}}_{s2}(\eta)$ are used to construct:

$$\boldsymbol{\mathcal{U}}_{s2} = \sum_{\eta=1}^{D} \vartheta_\eta \tilde{\boldsymbol{\mathcal{U}}}_{s2}(\eta) \tag{44}$$

where $\{\vartheta_\eta\}_{\eta=1}^{D}$ are a set of complex weighting factors. Analogous to (38),

$$\boldsymbol{\mathcal{U}}_{s1} \times_{D+1} (\boldsymbol{\Psi}_s)^T = \boldsymbol{\mathcal{U}}_{s2} \tag{45}$$

where

$$\boldsymbol{\Psi}_s = \boldsymbol{T} \boldsymbol{\Phi}_s \boldsymbol{T}^{-1} \tag{46}$$

where $\boldsymbol{T}$ denotes the nonsingular matrix to be determined and

$$\boldsymbol{\Phi}_s = diag \left(\begin{bmatrix} \psi_1 & \psi_2 & \cdots & \psi_D \end{bmatrix} \right) \tag{47}$$

where $\psi_\eta = \sum_{p=1}^{P} \vartheta_\eta e^{j\omega_{\eta,p}}$. In our study, an approximate minimization of the mean square frequency error [27] is employed. The suboptimum selection can be obtained via the optimization as follows:

$$\hat{\boldsymbol{\vartheta}} = \arg \max_{\boldsymbol{\vartheta}} \sum_{p_i=1}^{P-1} \sum_{p_j=p_i+1}^{P} \left\| \left(\boldsymbol{\rho}_{p_i}^T - \boldsymbol{\rho}_{p_j}^T \right) \boldsymbol{\vartheta} \right\|_2^2$$
$$= \arg \max_{\boldsymbol{\vartheta}} \boldsymbol{\vartheta}^H \boldsymbol{\Omega}^H \boldsymbol{\Omega} \boldsymbol{\vartheta} \tag{48}$$
$$s.t. \|\boldsymbol{\vartheta}\|_2 = 1$$

where

$$\boldsymbol{\Omega} = [\boldsymbol{\rho}_{1,2}, \boldsymbol{\rho}_{1,3}, \cdots, \boldsymbol{\rho}_{1,F}, \boldsymbol{\rho}_{2,3}, \cdots, \boldsymbol{\rho}_{P-1,P}]^T$$
$$\boldsymbol{\rho}_{p_i,p_j} = \boldsymbol{\rho}_{p_i}^T - \boldsymbol{\rho}_{p_j}^T \tag{49}$$
$$\boldsymbol{\rho}_p = [e^{j\omega_{1,p}}, e^{j\omega_{2,p}}, \cdots, e^{j\omega_{D,p}}]^T$$

It is evident that the solution of (48) can be given by the eigenvector corresponding to the largest eigenvalue of $\boldsymbol{\Omega}^H \boldsymbol{\Omega}$. Since $\boldsymbol{\Omega}$ is constructed by the unknown frequencies, iterative estimations of $\{\omega_{\eta,p}\}$ and ϑ are required. The initial each element of complex weighting factors ϑ satisfies that $|\vartheta_\eta| =$

$1/\sqrt{D}$ and the phase of ϑ_η is uniformly distributed within $[-\pi, \pi]$. The complete procedure of parameter estimation is summarized in Table II.

TABLE II
TENSOR GENERALIZED WEIGHTED LINEAR PREDICTOR BASED METHOD

1) Compute HOSVD of $\boldsymbol{\mathcal{Y}}$ to obtain $\boldsymbol{\mathcal{U}}_s$ in (24), and generate initial $\boldsymbol{\vartheta}$
For iter1=1,2,. . . ,ι do.
2) Construct $\boldsymbol{\mathcal{U}}_{s1}$ and $\boldsymbol{\mathcal{U}}_{s2}$ according to (38), (39) and (44), then compute $\boldsymbol{\Psi}_s = \left([\boldsymbol{\mathcal{U}}_{s1}]^T_{D+1}\right)^\dagger \left([\boldsymbol{\mathcal{U}}_{s2}]^T_{D+1}\right)$ from (45).
3) Perform eigenvalue decomposition on $\boldsymbol{\Psi}_s$ to obtain $\boldsymbol{T}_s$ of (46) and solve $\boldsymbol{\mathcal{G}}_s$ according to (28) as $[\boldsymbol{\mathcal{G}}_s]^T_{D+1} = [\boldsymbol{\mathcal{U}}_s]^T_{D+1}\,\boldsymbol{T}_s$.
4) For each p, extract subtensor $\boldsymbol{\mathcal{G}}_{sp}$ from $\hat{\boldsymbol{\mathcal{G}}}_s$ (25) and perform truncated HOSVD to obtain $\boldsymbol{\alpha}_p^{(\eta)}$ from (30).
5) For each $\boldsymbol{\alpha}_p^{(\eta)}$, compute the GWLP solution of $\{\hat{\omega}_{\eta,p}\}$ based on Table I.
6) Determine $\hat{\theta}_p, \hat{v}_p\ \Delta\hat{r}_p$, based on (15)-(17). Note that all the parameters are paired up.
7) Construct $\boldsymbol{\Omega}$ according to (49) and compute dominate eigenvector of $\boldsymbol{\Omega}^H\boldsymbol{\Omega}$ to get update $\boldsymbol{\vartheta}$.
End for

C. Identifiability

One significant indicator for joint parameter estimation methods is to determine the maximum number of resolvable components for a given sample size in the noiseless case, which is also referred to as the identifiability bound herein. The conventional identifiability bound provides a sufficient identification condition for multidimensional frequency estimation. In this section, the identifiability of the proposed TGWLP method for joint range-angle-velocity estimation of FDA-MIMO radar is analyzed.

The single-pulse-group measurement data during the qth pulse-group interval in (14) can be simply modeled as a constant modulus 3D HR problem:

$$\tilde{\mathcal{X}}_{n,m,l} = \sum_{p=1}^{P} \xi'_p e^{j(n_1-1)\omega_{1,p}} e^{j(n_2-1)\omega_{2,p}} e^{j(n_3-1)\omega_{3,p}} \quad (50)$$

which can be regarded as a typical 3D HR problem associated to the Swerling I target model. For the constant modulus 3D HR problem, it was proven in [39], that, if

$$P \le \left\lceil \frac{N_1}{2} \right\rceil \times \left\lceil \frac{N_2}{2} \right\rceil \times \left\lceil \frac{N_3}{2} \right\rceil \quad (51)$$

then the decomposition is almost surely unique, provided that the $3P$ frequencies $(\omega_{1,p}, \omega_{2,p}, \omega_{3,p})$, $p = 1, 2, ..., P$, are drawn from a jointly continuous distribution. Later on, this bound was relaxed in [19], where it was proven that, if

$$P \le \max_{\substack{N'_\eta + N''_\eta = N_\eta+1 \\ 1 \le N'_\eta \le N_\eta \\ 1 \le \eta \le 3}} \min\left\{2\prod_{\eta=1}^{3} N'_\eta, \prod_{\eta=1}^{3} N''_\eta\right\} \quad (52)$$

where $N'_\eta + N''_\eta = N_\eta + 1$, then the decomposition is almost surely unique, given that the frequencies $(\omega_{1,p}, \omega_{2,p}, \omega_{3,p})$, $p = 1, 2, ..., P$, are drawn from a jointly continuous distribution.

Since the multiple-pulse-group measurement data in (14) is modeled as a superposition of undamped exponentials sampled on a 3D grid at Q_g pulse-groups of intervals, the data is sampled on a four-dimensional lattice. In our work, the 3D

parameter estimation is casted into a multiple-pulse-group version of the 3D HR problem [24], which is associated to the mixed Swerling target model. It is assumed that the observed tensor is modified via FB averaging in (37) and spatial smoothing [19] as:

$$\mathcal{Y}_{smooth} \in \mathbb{C}^{N'_1 \times N'_2 \times \cdots \times N'_3 \times Q_g'} \quad (53)$$

where $Q_g' = 2Q_g \sum_{\eta=1}^{3} N''_\eta$. It was proven in [27], that, if

$$P \le \max_{\substack{N'_\eta + N''_\eta = N_\eta+1 \\ 1 \le N'_\eta \le N_\eta \\ 1 \le \eta \le 3}} \min\left\{\prod_{\eta=1}^{3}(N'_\eta - 1), 2Q_g\prod_{\eta=1}^{3} N''_\eta\right\} \quad (54)$$

then the decomposition in (14) is almost surely unique, given that the $3P$ frequencies $\{\omega_{\eta,p}\}_{\eta=1}^{3}$, and PQ_g coefficients $\{\xi_p(q)\}_{q=1}^{Q_g}$, $p = 1, 2, ..., P$, are assumed to be drawn from jointly continuous distributions with respect to the Lebesgue measure in $\mathbb{O}^{3P \times 1}$ and $\mathbb{C}^{PQ_g \times 1}$, respectively. $\mathbb{O}$ denotes as the set $(-\pi, \pi]$. That is, the range, angle and velocity can be unambiguously estimated if the following conditions are satisfied:

$$\begin{cases} |4\Delta r_p\Delta f - \cos(\theta_p)c| \le c \\ 4|v_p| \le \lambda_0 f_{PRF} \end{cases} \quad (55)$$

Furthermore, when $Q_g \le \frac{1}{2}\prod_{\eta=1}^{3}(N_\eta - 1)$, the identifiability bound is no greater than $\left\lfloor \frac{2Q_g\bar{N}}{\left(1+\sqrt[3]{2Q_g}\right)^3} \right\rfloor$; when $Q_g \ge \frac{1}{2}\prod_{\eta=1}^{3}(N_\eta - 1)$, the identifiability bound becomes a constant $\prod_{\eta=1}^{3}(N_\eta - 1)$ which is approximate to the data sample size of single pulse group, and there is no data smoothing in this case from the perspective of maximizing identifiability since $N''_\eta = 1$ and $N'_\eta = N_\eta$, for any η.

D. Performance Analysis

For fair comparison with the proposed method, the benchmark to assess the unbiased parameter estimators for FDA-MIMO radar is studied in terms of the Cramér-Rao bound (CRB). Consider the interference-free case, the CRBs for ranges, angle, and velocity can be expressed as:

$$D_v = \frac{1}{2QSNR}\frac{12}{N_1N_2N_3(N_3^2 - 1)\kappa_v^2} \quad (56)$$

$$D_\theta = \frac{1}{2QSNR}\frac{12}{N_1N_2N_3(N_2^2 - 1)\kappa_R^2} \quad (57)$$

$$D_r = \frac{1}{2QSNR}\frac{12(N_2^2 - 1)\kappa_R^2 + (N_1^2 - 1)\kappa_T^2}{N_1N_2N_3(N_1^2 - 1)(N_2^2 - 1)\kappa_r^2\kappa_R^2} \quad (58)$$

$$D_{\theta r} = \frac{1}{2QSNR}\frac{12\kappa_T}{N_1N_2N_3(N_2^2 - 1)\kappa_R^2\kappa_r} \quad (59)$$

$$D_{vr} = D_{v\theta} = 0 \quad (60)$$

The derivation of (56)-(60) is given in detail in Appendix, where the parameter estimation precision and the coupling between two parameters are given. Considering the colocated

MIMO radar with identical transmit and receive array elements, i.e., $N_1 = N_2$ and $d_R = d_T = d$. We obtain

$$D_v = \frac{1}{8QSNR} \frac{3\lambda_0^2}{\pi^2 N_1^2 N_3 (N_3^2 - 1) T_P^2} \tag{61}$$

$$D_\theta = \frac{1}{2QSNR} \frac{3\lambda_0^2}{\pi^2 N_1^2 N_3 (N_1^2 - 1) d^2 \sin^2(\theta)} \tag{62}$$

$$D_r = \frac{1}{4QSNR} \frac{3c^2}{\pi^2 N_1^2 N_3 (N_1^2 - 1) \Delta f^2} \tag{63}$$

$$D_{\theta r} = \frac{1}{4QSNR} \frac{3\lambda_0 c}{\pi^2 N_1^2 N_3 (N_1^2 - 1) d \sin(\theta) \Delta f} \tag{64}$$

Herein, the estimation precisions of radial velocity, the conic angle and slant range depend on the PRI, the array aperture and the frequency increment, respectively. It is observed that the estimation precisions of the velocity, the range, and the angle can be improved by increasing the number of snapshots, the frequency increment and the effective array aperture perpendicular to the direction of $\theta - 90°$, respectively. It is indicated from (64) that the coupling between range and angle parameters is dependent on the effective array aperture as well as the frequency increment. With the increment of the absolute value of $\theta - 90°$, the loss of the effective array aperture aggravates the coupling of range and angle, which leads to the angle estimation precision loss. Similarly, the smaller frequency increment also aggravates the coupling as well as degrades the range estimation precision.

V. SIMULATION RESULTS

In this section, the effectiveness of the proposed method is demonstrated along with the simulation parameters listed in Table III, where the frequency increment is optimally chosen according to [16]. Note that the transmit and receive arrays of FDA-MIMO radar share the ULA with the same elements, i.e., $N_1 = N_2$. The reflection coefficient of the pth target obeys the complex Gaussian distribution with zero mean and variance σ_p^2. The number of samples for each transmitted pulse is 512. Computer simulations to evaluate the performance of the proposed TGWLP and TGWLP-FB have been carried out by comparing with the unitary tensor ESPRIT (UTE) [19], and IMDF [27] schemes as well as CRB. In the following

TABLE III
PARAMETERS OF FDA-MIMO RADAR

Parameters	Value
Carrier frequency	5GHz
Frequency increment	301.25kHz
PRF	5kHz
Bandwidth	15MHz
Element number	9
Element spacing	0.03m
Sample number within pulse	6
Range ambiguity number	4
Maximum unambiguous range	30km
Range resolution	10m
The number of pulse groups	10
The number of pulse number within each group	10

experiments, 500 Monte Carlo trials are simulated and the corresponding root mean square error (RMSE) is defined as:

$$RMSE = \sqrt{\sum_{\varsigma=1}^{500} \sum_{p=1}^{P} \left\{ \left(\hat{\theta}_p^\varsigma - \theta_p^\varsigma \right)^2 + \left(\hat{v}_p^\varsigma - v_p^\varsigma \right)^2 + \left(\Delta \hat{r}_p^\varsigma - \Delta r_p^\varsigma \right)^2 \right\}} \tag{65}$$

where $\hat{\theta}_p^\varsigma$, v_p^ς and $\Delta \hat{r}_p^\varsigma$ denote the estimations of true angle, velocity and principal range difference, respectively, in the ςth trial.

Prior to the comparative simulations, the performance of the TGWLP-FB method under different combinations of iteration number ι and WLP/GWLP is firstly tested and the benchmark of CRB is also included. The target reflection coefficients are randomly generated with variances $\{1, 0.9, 0.95\}$. The ranges of the targets are identical. The index of range ambiguity of the targets is fixed at the same number. The principal range difference of the targets is a random variable uniformly distributed between $[-5m, 5m]$, but fixed and identical for the three targets on each trial. The conic angles of the targets are $[104°, 98°, 93°]$ and the velocities are chosen as $[35, 42, 53]\, m/s$. The root mean square error (RMSE) performance with respect to SNR is shown in Fig. 2. It is shown that the RMSEs drop sharply when the SNR changes from -25 to -20 dB. This is because the performance of estimators would be evidently degraded once SNR exceeds the threathold. The
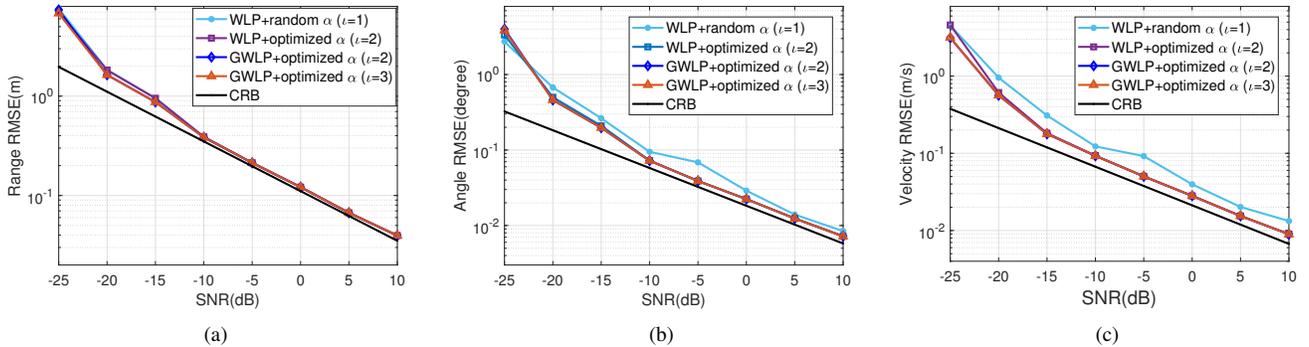

Fig. 2. RMSEs versus SNR in identical range case. (a) Range estimation. (b) Angle estimation. (c) Velocity estimation.

RMSE results reveal not only the optimized performance of the estimator but also the situation where the estimator breaks down. With the choice of WLP and random ϑ, the estimator suffers from the performance degradation. It is observed that both GWLP and optimized complex weighting factor improve the proposed estimator performance. With the combination of GWLP and $\iota = 2$ corresponding to optimized complex weighting factors, the proposed estimator is able to attain the CRB. Besides, no obvious improvement on estimation precision is observed for larger iteration number like $\iota = 3$. As a result, our proposed method adopts the combination of GWLP and $\iota = 2$ in the subsequent tests.

Then, the scattering result for TGWLP-FB method is further given in Fig. 3, where 500 Monte Carlo simulations have been carried out at $SNR = -5dB$. It is shown that the estimated points of the parameters are clustered and their cluster centers are very close to the true parameters along to each dimension. Besides, the overwhelming majority of estimated points are randomly distributed within narrow intervals. For each target, the three estimated parameters of each target are automatically paired without extra computation. As is shown in Fig.3, the range scattering results are bigger than other two results. This is because the estimation error of the principal range difference should be numerically larger than that of the angle and velocity according to (15)-(17). The estimation error of the principal range difference implicates the estimation error of the angle.
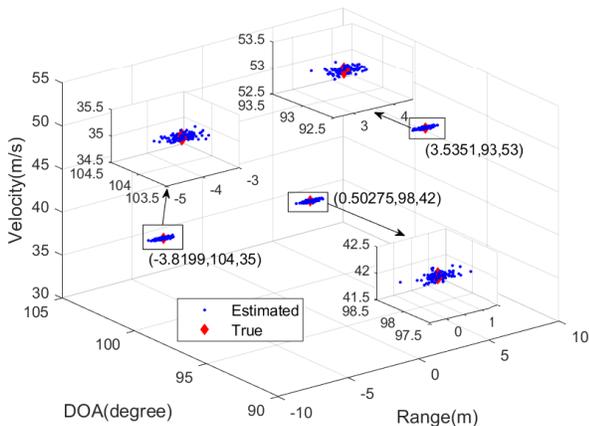
In the third simulation, the proposed methods are compared with the UTE, and IMDF schemes in identical range case, where the simulation settings are identical to those of the previous simulation. To this end, 500 Monte Carlo simulations have been carried out. The RMSEs and Average CPU time of different methods with respect to SNR are shown in Fig. 4. It is seen that the TGWLP-FB method has the best performance and its precision is close to the CRB. As expected, TGWLP-FB is able attain higher estimation precision than the standard TGWLP estimator. Furthermore, it is observed that proposed methods have great range estimation performance advantage over those of UTE and IMDF at sufficiently high SNR conditions ($SNR \geq -5dB$), which might be owing to the combination of complex weighting scheme for improved array steering tensor estimation and subspace based GWLP for improved frequency estimation. Although IMDF adopts the complex weighting optimization scheme, its performance is limited by the matrix pencil based algorithm. Besides, the average computation times of the UTE, IMDF, TGWLP and TGWLP-FB algorithms in a single run are measured as 0.029s, 2.181s, 0.012s and 0.025s, respectively, indicating the computational attractiveness of the TGWLP approach.

In the fourth simulation, the performance versus the number of array elements N_1 at $SNR = -5dB$ is examined and the complexity of the proposed approach is also evaluated. The index of range ambiguity of the targets is fixed at 1, and the principal range difference of the targets is a random variable uniformly distributed between $[-5m, 5m]$, but different for the three targets on each trial. All other parameter settings are identical to those of the previous simulation. The RMSEs and runtime results are shown in Fig. 5. As is shown in Figs. 5(a), (b) and (c), all the RMSEs of estimators reduce with the increasing N_1. The TGWLP-FB provides the best estimation performance among the methods compared. Fig. 5(d) shows that the complexities of TGWLP and TGWLP-FB slightly increase with larger N_1, while the complexity of IMDF rapidly increases. IMDF suffers from the heavy computational burden involved in the circular mean process. Although the UTE scheme is the most computationally attractive for small N_1, its complexity is higher than that of the TGWLP-FB algorithm for the large array aperture ($N_1 \geq 7$).

The final simulation is dedicated to the evaluation of the CRBs in the single target case at $SNR = -5dB$ with all other parameters set as table III. First, we examine the CRB for

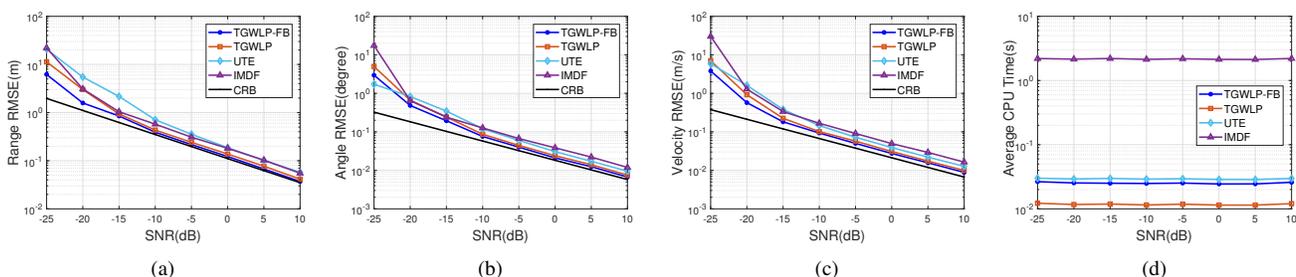Fig. 3. Scattering result for TGWLP-FB

Fig. 4. RMSEs and average CPU time of different methods with respect to SNR in identical range case. (a) Range estimation. (b) Angle estimation. (c) Velocity estimation. (d) Average CPU time per run.

angle versus the number of pulse groups. The signal of target is located at θ, varying with the angle separation $\Delta\theta = |\theta - 90°|$. As is shown in Fig. 6(a), increasing $\Delta\theta$ hampers the performance of FDA-MIMO radar with fixed array aperture in angle estimation. Then the CRB for coupling of range and angle is considered. As is shown in Fig. 6(b), the root CRB for coupling between range and angle varies with pulse groups and $\Delta\theta$ which is noted to associate with the effective array aperture. For FDA-MIMO radar with fixed array aperture, the coupling is aggravated by both of the larger $\Delta\theta$ and the smaller pulse groups.
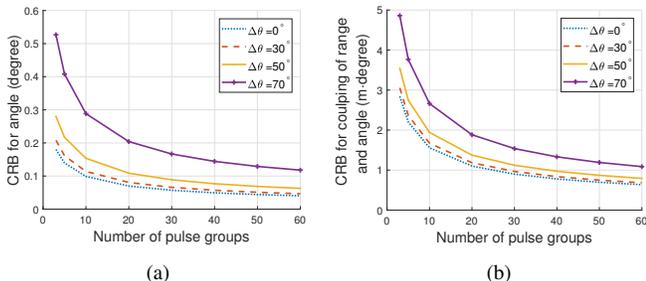

Fig. 6. CRB versus pulse groups. (a) The angle estimation. (b) The coupling of range and angle.

VI. CONCLUSION

In this paper, tensor modeling of multidimensional FDA-MIMO radar signal is developed, so that the joint parameter estimation is casted into multiple-pulse-group version of 3D HR problem associated to the mixed Swerling model rather than the typical 3D HR problem associated to the Swerling I model. In the mixed Swerling case, the RCS of the target should be constant within each pulse group but varying among different pulse groups. Pulse-group diversity is exploited to obtain precise velocity estimation. Unambiguous range estimation can be obtained by range dependence compensation. In order to improve the parameter estimation of targets with some identical parameters, TGWLP is proposed which employs the combination of complex weighting scheme for improved array steering tensor estimation and subspace based GWLP for improved frequency estimation. The final estimation of unambiguous slant range, conic angle, and radial velocity of a moving target can be easily obtained with all the parameter

pairing automatically achieved, which is free of the extra burden from pairing process. Furthermore, the identifiability of the proposed method for joint parameter estimation is analyzed and compared with other similar methods. Our analysis is based on the multiple-pulse-group version of 3D HR problem associated to the mixed Swerling model, rather than typical 3D HR problem associated to the Swerling I model. It is shown that the identifiability bound should increase as the number of pulse groups increases until it reaches a threshold. Additionally, CRBs for angle, range, and velocity are derived, which are the common benchmarks to assess the unbiased estimators for FDA-MIMO radar. Finally, numerical simulations show the superiority of proposed TGWLP method in terms of accuracy and computational cost compared to existing methods.

APPENDIX

In this section, we analyze the performance lower bound of joint parameter estimation for the FDA-MIMO radar by deriving the CRBs for the velocity, range and angle. The derivation can regarded as the 3D extension of the CRBs for the range and angle [14], [16]. The unknown parameter vector can be written as:

$$
\begin{aligned}
\Psi &= \left[\boldsymbol{\alpha}^T, \boldsymbol{\beta}^T \right] \\
&= \left[v, r, \theta, \bar{\xi}, \breve{\xi}, \sigma \right]^T
\end{aligned} \tag{66}
$$

where σ denotes the zero-mean complex Gaussian white noise parameter with spatial covariance $\boldsymbol{R}_N$, and the parameters of the target are gathered in $\boldsymbol{\alpha} = \left[v, r, \theta, \bar{\xi}, \breve{\xi} \right]^T$, where $\bar{\xi} = \mathrm{Re}\{\xi\}$ and $\breve{\xi} = \mathrm{Im}\{\xi\}$. Since the parameters of interest and nuisance are decoupled, the Fisher information matrix (FIM) [40] for the parameters of interest is

$$
\boldsymbol{F} = \frac{2QE}{N_1 \sigma^2} \mathrm{Re}\left\{ \left(\frac{\partial \xi \boldsymbol{u}(v, r, \theta)}{\partial \boldsymbol{\alpha}} \right)^H \left(\frac{\partial \xi \boldsymbol{u}(v, r, \theta)}{\partial \boldsymbol{\alpha}} \right) \right\} \tag{67}
$$

where $\boldsymbol{u}(v, r, \theta) = \boldsymbol{c}(v) \otimes \boldsymbol{b}(\theta) \otimes \boldsymbol{a}(\tilde{r}, \theta)$ is the joint transmit-receive steering vector of the target after compensation, and $\boldsymbol{c}(v) = [1, e^{j 4\pi v T_p / \lambda_0}, \ldots, e^{j(N_3-1)4\pi v T_p / \lambda_0}]$. Define three auxiliary vectors as:

$$
\boldsymbol{u}_v = \partial \boldsymbol{u} / \partial v = \frac{\partial \boldsymbol{c}(v)}{\partial v} \otimes \boldsymbol{b}(\theta) \otimes \boldsymbol{a}(r - \rho, \theta) \tag{68}
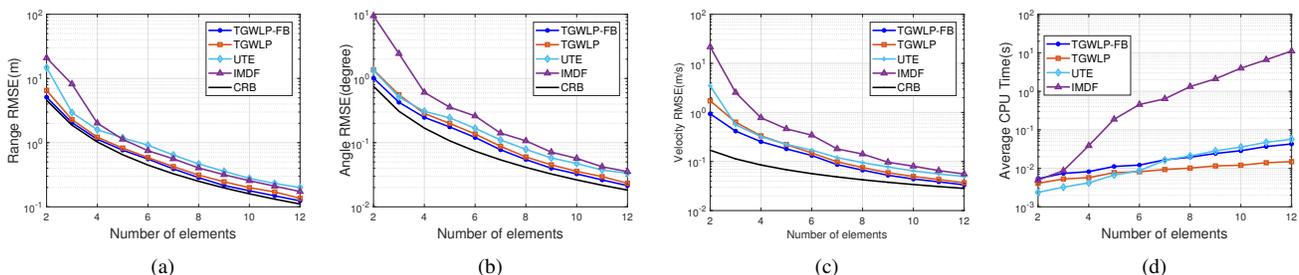$$

Fig. 5. RMSEs and average CPU time of different methods with respect to N_1 in different range case. (a) Angle estimation. (b) Range estimation. (c) Velocity estimation. (d) Average CPU time per run.

$$\boldsymbol{u}_\theta = \partial\boldsymbol{u}/\partial\theta = \boldsymbol{c}(v) \otimes \frac{\partial\boldsymbol{b}(\theta)}{\partial\theta} \otimes \boldsymbol{a}(r-\rho,\theta)$$
$$+ \boldsymbol{c}(v) \otimes \boldsymbol{b}(\theta) \otimes \left(\boldsymbol{r}(r-\rho) .* \frac{\partial\boldsymbol{d}(\theta)}{\partial\theta}\right) \tag{69}$$

$$\boldsymbol{u}_r = \partial\boldsymbol{u}/\partial r = \boldsymbol{c}(v) \otimes \boldsymbol{b}(\theta) \otimes \left(\frac{\partial\boldsymbol{r}(r-\rho)}{\partial r} .* \boldsymbol{d}(\theta)\right) \tag{70}$$

where the three auxiliary vectors can be explicitly expressed as:

$$\frac{\partial\boldsymbol{c}(v)}{\partial v} = j\kappa_v \boldsymbol{E_g}\boldsymbol{c}(v), \kappa_v = 4\pi T_P/\lambda_0 \tag{71}$$

$$\frac{\partial\boldsymbol{b}(\theta)}{\partial\theta} = -j\kappa_R \boldsymbol{E_b}\boldsymbol{b}(\theta), \kappa_R = 2\pi d_R \sin(\theta)/\lambda_0 \tag{72}$$

$$\frac{\partial\boldsymbol{d}(\theta)}{\partial\theta} = -j\kappa_T \boldsymbol{E_d}\boldsymbol{d}(\theta), \kappa_T = 2\pi d_T \sin(\theta)/\lambda_0 \tag{73}$$

$$\frac{\partial\boldsymbol{r}(r)}{\partial r} = -j\kappa_r \boldsymbol{E_r}\boldsymbol{r}(r), \kappa_r = 4\pi\Delta f/c \tag{74}$$

$$\boldsymbol{E_r} = \boldsymbol{E_d} = diag\left([0,1,\ldots,N_1-1]^T\right) \tag{75}$$

$$\boldsymbol{E_b} = diag\left([0,1,\ldots,N_2-1]^T\right) \tag{76}$$

$$\boldsymbol{E_c} = diag\left([0,1,\ldots,N_3-1]^T\right) \tag{77}$$

Using the Schur complement, the FIM can be expressed as:

$$\boldsymbol{F} = \frac{2QE|\xi|^2}{N_1\sigma^2}\begin{bmatrix} \boldsymbol{F}_{11} & \boldsymbol{F}_{12} \\ \boldsymbol{F}_{21} & \boldsymbol{F}_{22} \end{bmatrix}^{-1} = \frac{2QE|\xi|^2}{N_1\sigma^2}\begin{bmatrix} \boldsymbol{G} & \times \\ \times & \times \end{bmatrix} \tag{78}$$

where the four block matrix in (77) can be expressed as

$$\boldsymbol{F}_{11} = \begin{bmatrix} \|\boldsymbol{u}_v\|^2 & \mathrm{Re}\{\boldsymbol{u}_v\boldsymbol{u}_\theta\} & \mathrm{Re}\{\boldsymbol{u}_v\boldsymbol{u}_r\} \\ \mathrm{Re}\{\boldsymbol{u}_v\boldsymbol{u}_\theta\} & \|\boldsymbol{u}_\theta\|^2 & \mathrm{Re}\{\boldsymbol{u}_\theta\boldsymbol{u}_r\} \\ \mathrm{Re}\{\boldsymbol{u}_v\boldsymbol{u}_r\} & \mathrm{Re}\{\boldsymbol{u}_\theta\boldsymbol{u}_r\} & \|\boldsymbol{u}_r\|^2 \end{bmatrix} \tag{79}$$

$$\boldsymbol{F}_{12} = \boldsymbol{F}_{21}^T = \begin{bmatrix} \mathrm{Re}\{\boldsymbol{u}_v^H\boldsymbol{u}\} & -\mathrm{Im}\{\boldsymbol{u}_v^H\boldsymbol{u}\} \\ \mathrm{Re}\{\boldsymbol{u}_\theta^H\boldsymbol{u}\} & -\mathrm{Im}\{\boldsymbol{u}_\theta^H\boldsymbol{u}\} \\ \mathrm{Re}\{\boldsymbol{u}_r^H\boldsymbol{u}\} & -\mathrm{Im}\{\boldsymbol{u}_r^H\boldsymbol{u}\} \end{bmatrix} \tag{80}$$

$$\boldsymbol{F}_{22} = \left[\|\boldsymbol{u}\|^2\boldsymbol{I}_2\right] \tag{81}$$

and $\boldsymbol{G}$ can be expressed as (82). Note that

$$\|\boldsymbol{u}\|^2 = N_1N_2N_3 \tag{83}$$

$$\|\boldsymbol{u}_v\|^2 = \kappa_v^2 N_1N_2 \sum_{n_3=1}^{N_3}(n_3-1)^2 \tag{84}$$

$$\|\boldsymbol{u}_\theta\|^2 = 2\kappa_T\kappa_R N_3 \sum_{n_2=1}^{N_2}(n_2-1)\sum_{n_1=1}^{N_1}(n_1-1)$$
$$+ \kappa_R^2 N_1N_3 \sum_{n_2=1}^{N_2}(n_2-1)^2 + \kappa_T^2 N_2N_3 \sum_{n_1=1}^{N_1}(n_1-1)^2 \tag{85}$$

$$\|\boldsymbol{u}_r\|^2 = \kappa_r^2 N_2N_3 \sum_{n_1=1}^{N_1}(n_1-1)^2 \tag{86}$$

$$\boldsymbol{u}_v^H\boldsymbol{u} = -j\kappa_v N_1N_2 \sum_{n_3=1}^{N_3}(n_3-1) \tag{87}$$

$$\boldsymbol{u}_r^H\boldsymbol{u} = j\kappa_r N_2N_3 \sum_{n_1=1}^{N_1}(n_1-1) \tag{88}$$

$$\boldsymbol{u}_\theta^H\boldsymbol{u} = j\left[\kappa_R N_1N_3 \sum_{n_2=1}^{N_2}(n_2-1) + \kappa_T N_2N_3 \sum_{n_1=1}^{N_1}(n_1-1)\right] \tag{89}$$

$$\boldsymbol{u}_v^H\boldsymbol{u}_\theta = -\kappa_v \sum_{n_3=1}^{N_3}(n_3-1)$$
$$\times \left[\kappa_R N_1 \sum_{n_2=1}^{N_2}(n_2-1)d + \kappa_T N_2 \sum_{n_1=1}^{N_1}(n_1-1)\right] \tag{90}$$

$$\boldsymbol{u}_v^H\boldsymbol{u}_r = -\kappa_v\kappa_r N_2 \sum_{n_1=1}^{N_1}(n_1-1)\sum_{n_3=1}^{N_3}(n_3-1) \tag{91}$$

$$\boldsymbol{u}_\theta^H\boldsymbol{u}_r = \kappa_r N_3$$
$$\times \left[\kappa_R \sum_{n_2=1}^{N_2}(n_2-1)\sum_{n_1=1}^{N_1}(n_1-1) + \kappa_T N_2 \sum_{n_1=1}^{N_1}(n_1-1)^2\right] \tag{92}$$

Substituting (83)-(92) into (82) yields

$$G_{11} = \frac{N_1N_2N_3\left(N_3^2-1\right)\kappa_v^2}{12} \tag{93}$$

$$G_{22} = \frac{N_1N_2N_3\left[\left(N_2^2-1\right)\kappa_R^2 + \left(N_1^2-1\right)\kappa_T^2\right]}{12} \tag{94}$$

$$G_{33} = \frac{N_1N_2N_3\left(N_1^2-1\right)\kappa_r^2}{12} \tag{95}$$

$$G_{23} = G_{32} = \frac{N_1N_2N_3\left(N_1^2-1\right)\kappa_T\kappa_r}{12} \tag{96}$$

$$G_{12} = G_{21} = G_{13} = G_{31} = 0 \tag{97}$$

$$\det(\boldsymbol{G}) = \frac{\kappa_v^2\kappa_R^2\kappa_r^2 N_1^3N_2^3N_3^3\left(N_1^2-1\right)\left(N_2^2-1\right)\left(N_3^2-1\right)}{1728} \tag{98}$$

$$\boldsymbol{G} = \boldsymbol{F}_{11} - \boldsymbol{F}_{12}\boldsymbol{F}_{22}^{-1}\boldsymbol{F}_{21}$$
$$= \begin{bmatrix} \|\boldsymbol{u}_v\|^2 - \frac{|\boldsymbol{u}_v^H\boldsymbol{u}|^2}{\|\boldsymbol{u}\|^2} & \mathrm{Re}\{\boldsymbol{u}_v^H\boldsymbol{u}_\theta\} - \frac{\mathrm{Re}\{\boldsymbol{u}^H\boldsymbol{u}_v\boldsymbol{u}_\theta^H\boldsymbol{u}\}}{\|\boldsymbol{u}\|^2} & \mathrm{Re}\{\boldsymbol{u}_v^H\boldsymbol{u}_r\} - \frac{\mathrm{Re}\{\boldsymbol{u}^H\boldsymbol{u}_v\boldsymbol{u}_r^H\boldsymbol{u}\}}{\|\boldsymbol{u}\|^2} \\ \mathrm{Re}\{\boldsymbol{u}_v^H\boldsymbol{u}_\theta\} - \frac{\mathrm{Re}\{\boldsymbol{u}^H\boldsymbol{u}_v\boldsymbol{u}_\theta^H\boldsymbol{u}\}}{\|\boldsymbol{u}\|^2} & \|\boldsymbol{u}_\theta\|^2 - \frac{|\boldsymbol{u}_\theta^H\boldsymbol{u}|^2}{\|\boldsymbol{u}\|^2} & \mathrm{Re}\{\boldsymbol{u}_\theta^H\boldsymbol{u}_r\} - \frac{\mathrm{Re}\{\boldsymbol{u}^H\boldsymbol{u}_\theta\boldsymbol{u}_r^H\boldsymbol{u}\}}{\|\boldsymbol{u}\|^2} \\ \mathrm{Re}\{\boldsymbol{u}_v^H\boldsymbol{u}_r\} - \frac{\mathrm{Re}\{\boldsymbol{u}^H\boldsymbol{u}_v\boldsymbol{u}_r^H\boldsymbol{u}\}}{\|\boldsymbol{u}\|^2} & \mathrm{Re}\{\boldsymbol{u}_\theta^H\boldsymbol{u}_r\} - \frac{\mathrm{Re}\{\boldsymbol{u}^H\boldsymbol{u}_\theta\boldsymbol{u}_r^H\boldsymbol{u}\}}{\|\boldsymbol{u}\|^2} & \|\boldsymbol{u}_r\|^2 - \frac{|\boldsymbol{u}_r^H\boldsymbol{u}|^2}{\|\boldsymbol{u}\|^2} \end{bmatrix} \tag{82}$$

The closed-form CRBs for angle, range and velocity are

$$D_v = \frac{\det(M_{11})}{2QSNR\det(G)} \tag{99}$$

$$D_\theta = \frac{\det(M_{22})}{2QSNR\det(G)} \tag{100}$$

$$D_r = \frac{\det(M_{33})}{2QSNR\det(G)} \tag{101}$$

$$D_{\theta r} = \frac{\det(M_{23})}{2QSNR\det(G)} \tag{102}$$

$$D_{vr} = D_{v\theta} = 0 \tag{103}$$

where $\det(G)$ is the determinant of G, M_{ij} denotes the cofactor of $G_{i,j}$ which is the element in the ith row and jth colomn of G, $SNR = \left(E|\xi|^2/N_1\sigma^2\right)$. Therefore, (56)-(60) can be easily obtained according to (99)-(103). It is also indicated from (103) that there is no coupling between velocity and range/angle parameters.

REFERENCES

[1] M. N. El Korso, R. Boyer, A. Renaux, and S. Marcos, "Statistical resolution limit for source localization with clutter interference in a MIMO radar context," *IEEE Trans. Signal Process.*, vol. 60, no. 2, pp. 987–992, 2011.

[2] Z. Cheng, B. Liao, Z. He, J. Li, and J. Xie, "Joint design of the transmit and receive beamforming in mimo radar systems," *IEEE Trans. Veh. Technol.*, vol. 68, no. 8, pp. 7919–7930, 2019.

[3] L. Li, K. Ota, and M. Dong, "Humanlike driving: Empirical decision-making system for autonomous vehicles," *IEEE Trans. Veh. Technol.*, vol. 67, no. 8, pp. 6814–6823, 2018.

[4] I. Bilik, O. Longman, S. Villeval, and J. Tabrikian, "The rise of radar for autonomous vehicles: Signal processing solutions and future research directions," *IEEE Signal Process. Mag.*, vol. 36, no. 5, pp. 20–31, 2019.

[5] P. Baizert, T. B. Hale, M. A. Temple, and M. C. Wicks, "Forward-looking radar GMTI benefits using a linear frequency diverse array," *Electron. Lett.*, vol. 42, no. 22, pp. 1311–1312, 2006.

[6] W.-Q. Wang, "Range-angle dependent transmit beampattern synthesis for linear frequency diverse arrays," *IEEE Trans. Antennas Propag.*, vol. 61, no. 8, pp. 4073–4081, 2013.

[7] T. Eker, S. Demir, and A. Hizal, "Exploitation of linear frequency modulated continuous waveform (LFMCW) for frequency diverse arrays," *IEEE Trans. Antennas Propag.*, vol. 61, no. 7, pp. 3546–3553, 2013.

[8] P. Antonik, M. C. Wicks, H. D. Griffiths, and C. J. Baker, "Multi-mission multi-mode waveform diversity," in *Proc. IEEE Radar Conf.*, 2006, pp. 580–582.

[9] A. Basit, W. Wang, and S. Y. Nusenu, "Adaptive transmit beamspace design for cognitive FDA radar tracking," *IET Radar Sonar Navig.*, vol. 13, no. 12, pp. 2083–2092, 2019.

[10] G. M. Cleetus, "Properties of staggered PRF radar spectral components," *IEEE Trans. Aerosp. Electron. Syst.*, vol. 12, no. 6, pp. 800–803, 1976.

[11] K. Gerlach and G. Andrews, "Cascaded detector for multiple high-PRF pulse doppler radars," *IEEE Trans. Aerosp. Electron. Syst.*, vol. 26, no. 5, pp. 754–767, 1990.

[12] Y. Yang and R. S. Blum, "Phase synchronization for coherent MIMO radar: Algorithms and their analysis," *IEEE Trans. Signal Process.*, vol. 59, no. 11, pp. 5538–5557, 2011.

[13] W.-Q. Wang and H.-C. So, "Transmit subaperturing for range and angle estimation in frequency diverse array radar," *IEEE Trans. Signal Process.*, vol. 62, no. 8, pp. 2000–2011, 2014.

[14] J. Xiong, W.-Q. Wang, and K. Gao, "FDA-MIMO radar range–angle estimation: CRLB, MSE, and resolution analysis," *IEEE Trans. Aerosp. Electron. Syst.*, vol. 54, no. 1, pp. 284–294, 2017.

[15] M. Zatman, "The applicability of GMTI MIMO radar," in *Proc. IEEE Asilomar Conf. Signals, Syst. and Comput.*, 2010, pp. 2138–2142.

[16] J. Xu, G. Liao, S. Zhu, L. Huang, and H. C. So, "Joint range and angle estimation using MIMO radar with frequency diverse array," *IEEE Trans. Signal Process.*, vol. 63, no. 13, pp. 3396–3410, 2015.

[17] J. Xu, G. Liao, Y. Zhang, H. Ji, and L. Huang, "An adaptive range-angle-doppler processing approach for FDA-MIMO radar using three-dimensional localization," *IEEE J. Sel. Topics Signal Process.*, vol. 11, no. 2, pp. 309–320, 2016.

[18] J. Xu, W.-Q. Wang, C. Cui, and R. Gui, "Joint range, angle and doppler estimation for FDA-MIMO radar," in *Proc. IEEE Sensor Array Multi. Signal Process. Workshop*, 2018, pp. 499–503.

[19] M. Haardt, F. Roemer, and G. Del Galdo, "Higher-order SVD-based subspace estimation to improve the parameter estimation accuracy in multidimensional harmonic retrieval problems," *IEEE Trans. Signal Process.*, vol. 56, no. 7, pp. 3198–3213, 2008.

[20] L. De Lathauwer, B. De Moor, and J. Vandewalle, "A multilinear singular value decomposition," *SIAM J. Matrix Anal. Appl.*, vol. 21, no. 4, pp. 1253–1278, 2000.

[21] X. Liang, Y. Qian, Q. Guo, H. Cheng, and J. Liang, "AF: An association-based fusion method for multi-modal classification," *IEEE Transactions on Pattern Analysis and Machine Intelligence*, pp. 1–1, 2021.

[22] W. Sun and H.-C. So, "Accurate and computationally efficient tensor-based subspace approach for multidimensional harmonic retrieval," *IEEE Trans. Signal Process*, vol. 60, no. 10, pp. 5077–5088, 2012.

[23] P. Stoica, R. L. Moses *et al.*, *Spectral analysis of signals*. Upper Saddle River, NJ, USA: Prentice-Hall, 2005.

[24] D. Nion and N. D. Sidiropoulos, "Tensor algebra and multidimensional harmonic retrieval in signal processing for MIMO radar," *IEEE Trans. Signal Process.*, vol. 58, no. 11, pp. 5693–5705, 2010.

[25] M. Haardt and J. A. Nossek, "Simultaneous schur decomposition of several nonsymmetric matrices to achieve automatic pairing in multidimensional harmonic retrieval problems," *IEEE Trans. Signal Process.*, vol. 46, no. 1, pp. 161–169, 1998.

[26] J. Liu and X. Liu, "An eigenvector-based approach for multidimensional frequency estimation with improved identifiability," *IEEE Trans. Signal Process.*, vol. 54, no. 12, pp. 4543–4556, 2006.

[27] J. Liu, X. Liu, and X. Ma, "Multidimensional frequency estimation with finite snapshots in the presence of identical frequencies," *IEEE Trans. Signal Process.*, vol. 55, no. 11, pp. 5179–5194, 2007.

[28] W. G. Tang, H. Jiang, and Q. Zhang, "Range-angle decoupling and estimation for FDA-MIMO radar via atomic norm minimization and accelerated proximal gradient," *IEEE Signal Process Lett.*, vol. 27, pp. 366–370, 2020.

[29] C. Wen, J. Peng, Y. Zhou, and J. Wu, "Enhanced three-dimensional joint domain localized STAP for airborne FDA-MIMO radar under dense false-target jamming scenario," *IEEE Sensors J.*, vol. 18, no. 10, pp. 4154–4166, 2018.

[30] C. Zhou, Q. Liu, and X. Chen, "Parameter estimation and suppression for DRFM-based interrupted sampling repeater jammer," *IET Radar Sonar Navig.*, vol. 12, no. 1, pp. 56–63, 2017.

[31] J. Vandewalle, "Signal processing based on multilinear algebra," Ph.D. dissertation, K. U. Leuven, 1997.

[32] Y. Zhang, Z. Li, B. Cheong, H. Suarez, Y.-R. Huang, W. Blake, T. Yong, and J. Andrews, "Optimized radar signal processing for a low-cost, solid-state airborne radar," in *Proc. 36th Conf. Radar Meteorology*, 2013, pp. 16–20.

[33] X. Tan, W. Roberts, J. Li, and P. Stoica, "Range-doppler imaging via a train of probing pulses," *IEEE Trans. Signal Process.*, vol. 57, no. 3, pp. 1084–1097, 2008.

[34] J. Liu and X. Liu, "An eigenvector-based approach for multidimensional frequency estimation with improved identifiability," *IEEE Trans. Signal Process.*, vol. 54, no. 12, pp. 4543–4556, 2006.

[35] F. Roemer, H. Becker, M. Haardt, and M. Weis, "Analytical performance evaluation for hosvd-based parameter estimation schemes," in *Proc. 3rd IEEE Int. Workshop on Computational Advances in Multi-Sensor Adaptive Process.*, 2009, pp. 77–80.

[36] H.-C. So and F. K. Chan, "A generalized weighted linear predictor frequency estimation approach for a complex sinusoid," *IEEE Trans. Signal Process.*, vol. 54, no. 4, pp. 1304–1315, 2006.

[37] S. Kay, "A fast and accurate single frequency estimator," *IEEE Trans. Acoust., Speech, Signal Process.*, vol. 37, no. 12, pp. 1987–1990, 1989.

[38] G. H. Golub and C. F. van Loan, *Matrix Computations*, 4, Ed. Baltimore, MD, USA: The John Hopkins Univ. Press, 2013.

[39] X. Liu and N. D. Sidiropoulos, "Almost sure identifiability of constant modulus multidimensional harmonic retrieval," *IEEE Trans. Signal Process.*, vol. 50, no. 9, pp. 2366–2368, 2002.

[40] P. Stoica and A. Nehorai, "Music, maximum likelihood, and cramer-rao bound," *IEEE Trans. Acoust., Speech, Signal Process.*, vol. 37, no. 5, pp. 720–741, 1989.

Chao Wen received Ph.D degree in electrical circuit and system from Xidian University, Xi'an, China, in 2017. From 2017 to 2018, he was a principal investigator with the 723 Institute of China Shipbuilding Industry Corporation (CSIC), Yangzhou. He is currently a teacher with the Institute of Big Data Science and Industry, Shanxi University, Taiyuan, China. His research interests include artificial signal processing and neural networks.

Yu Xie received the Ph.D. degree in pattern recognition and intelligent systems from Xidian University, Xi'an, China, in 2020. From 2019 to 2020, he was a research assistant with School of Computer Science and Engineering, Nanyang Technological University, Singapore. He is currently a teacher with School of Computer and Information Technology, Shanxi University, Taiyuan, China. His research interests include graph neural networks and artificial intelligence security.

Zhiwei Qiao received the M.S. and Ph.D. degrees from North University of China, Taiyuan, Shanxi, China, in 2004, and from Beijing Jiaotong University, Beijing, China, in 2011, respectively. He is currently a Professor with School of Computer and Information Technology, Shanxi University, Taiyuan, Shanxi, China. He focuses on medical imaging and electron paramagnetic resonance imaging. He is the associate editor of CT theory and applications. He has authored over 50 articles on image reconstruction.

Liyun Xu received the Ph.D degree in applied mathematics from Beijing Institute of Technology, China, in 2018. She is currently a lecturer with the Institute of Big Data Science and Industry, Shanxi University, China. Her research interests include signal processing, machine learning and artificial intelligence.

Yuhua Qian received the M.S. and Ph.D. degrees from Shanxi University, Taiyuan, China, in 2005 and 2011, respectively. He is currently a Professor with the Key Laboratory of Computational Intelligence and Chinese Information Processing of Ministry of Education, Shanxi University. He is best known for multigranulation rough sets in learning from categorical data and granular computing. He is involved in research on pattern recognition, feature selection, rough set theory, granular computing, and artificial intelligence. He has authored over 100 articles on these topics in international journals and coferences. He served on the Editorial Board of the International Journal of Knowledge-Based Organizations and Artificial Intelligence Research. He has served as the Program Chair or Special Issue Chair of the Conference on Rough Sets and Knowledge Technology, the Joint Rough Set Symposium, and the Conference on Industrial Instrumentation and Control, and PC Members of many machine learning, data mining, and granular computing conferences.